Stony Brook University

The use of biomaterials for cell function enhancement: acceleration of fibroblast migration and promotion of stem cell proliferation

A Dissertation Presented

by

Sisi Qin

to

The Graduate School

in Partial Fulfillment of the

Requirements

for the Degree of

Doctor of Philosophy

in

Materials Sciences and Engineering

Stony Brook University

December 2014

Stony Brook University

The Graduate School

Sisi Qin

We, the dissertation committee for the above candidate for the

Doctor of Philosophy degree, hereby recommend

acceptance of this dissertation.

Dr. Miriam Rafailovich – Dissertation Advisor
Distinguished Professor of Department of Materials Science and Engineering
Stony Brook University

Dr. Dilip Gersappe - Chairperson of Defense
Professor of Department of Materials Science and Engineering
Stony Brook University

Dr. Richard Clark
Professor of Department of Biomedical Engineering
Stony Brook University

Dr. Marcia Simon
Professor of Department of Oral Biology and Pathology
Stony Brook University

This dissertation is accepted by the Graduate School

Charles Taber
Dean of the Graduate School

Abstract of the Dissertation

The use of biomaterials for cell function enhancement: acceleration of fibroblast migration and promotion of stem cell proliferation

by

Sisi Qin

Doctor of Philosophy

in

Materials Sciences and Engineering

Stony Brook University

2014

Abstract:

Wound healing and tissue regeneration proceed via fibroblast migration along three dimensional scaffolds composed of fibers with different diameters, spacing, and junction angles. In order to understand how each of these factors influences fibroblast migration, a technique for preparation of three dimensional fibrillar scaffolds was developed where the fiber diameters and the angles between adjacent fiber layers could be precisely controlled. In order to study the en-mass migration process, the agarose droplet method was chosen since it enabled accurate determinations of the dependence of the migration speed, focal adhesion distribution, and nuclear deformation on the fiber structures. Results showed that on oriented single fiber layers, if the fiber diameters exceeded 1μm, large focal adhesion complexes formed in a linear arrangement along the fiber axis and cell motion was highly correlated. For fibers 1μm or less,

some cell alignment along the fiber direction was measured, but no correlation between the distribution of focal adhesion points and fiber orientation was found.

On multi layered scaffolds the focal adhesion sites were found to concentrate at the junction points and the migration speed followed a parabolic function with a distinct minimum at 35°. When compared to fibroblasts plated on 90° fibers, fibroblasts plated on 30° fibers showed a decrease of 25% in the degree of nuclear deformation and an increase of 25% in the number of focal adhesion sites, indicating that cell migration speed was correlated to the angle and distance of approach to the junction point.

The time dependence of the migration velocity on oriented fibers was measured for four days and compared to the value measured on flat surfaces. After the initial 24 hour incubation period, the cells on both the 8μm fibers and flat surfaces migrated with a similar speed. During the next three days the migration speed for the cells on the fibrillar surfaces doubled in magnitude, while remained constant for the cells on the flat surfaces. The increased speed on the 8μm fiber surfaces could be correlated with a 20% increase in the nuclear deformation, and a decrease around 30% in the number of focal adhesion during the same observation period. RNA expression of Myosin IIA, a protein which complexes to the actin and is responsible for exertion of traction forces during migration was not upregulated during this process. On the other hand, histochemical staining of Myosin IIA showed that the protein had re-organized into large fibers which spanned the length of the cells. Observation of the cell morphology indicated that a new mode of motion had been established. Rather than the classical retraction of the cytoplasm followed by center of mass translation, which was observed on the flat surfaces, the cells were now moving by a contractile motion around the nucleus similar to that found in muscular motion. This mode was found to be more efficient when undergoing oriented motion.

In addition to orientation, surface mechanics are also important in the tissue regeneration process. This study demonstrated that mechanical factors are important for the maintenance of pluripotency and control of proliferation rates. CD34+ hematopoietic stem cells (HSCs) were transduced with ICD (intracellular domain)-Notch and plated on gelatin hydrogels, whose moduli were controlled by the crosslinking ratio. On the softer hydrogel, a synergy was achieved which resulted in more than a five-fold increase in proliferation and a four-fold increase in the preservation of stemness, while HSCs maintained their ability to differentiate into multiple blood cell lineages. These results point the way for achieving clinically significant expansion of human HSCs.

Table of Contents

List of Figures

List of Abbreviation

PMMA	Poly(methyl methacrylate)
DiD	1, 1′- dioctadecyl-3, 3, 3′, 3′-tetramethylindodicarbocyanine perchlorate
SEM	Scanning Electron Microscopy
FN	Fibronectin
DAPI	4’,6-diamiadino-2-phenylindole
HSC	Hematopoietic Stem Cell
TCP	Tissue Culture Petric Dish
CFU	Colony Forming Unit

Acknowledgments

I would have never been able to finish my dissertation without the guidance of my committee members, help from my friends, and support from my family.

I want to first show my greatest gratitude to my thesis advisor, Professor Miriam Rafailovich, who I will always remember for all the help and guidance she gave me throughout my Ph.D. study. Her kindness and support will continuously motivated me in my future path.

I would also like to present my deepest appreciation to Dr. Richard Clark, who generously provides the knowledgeable and resourceful working environment for the cell migration study. He has truly been a great mentor whom I can always look up to.

I am very grateful to Professor Marcia Simon and Professor Dilip Gersappe for their endless support and constructive criticism. Those advises have helped me breakthrough many obstacles during the research. Many thanks go to Dr. Jerell Aguila who did the amazing job on hematopoietic stem cell and the notch signaling pathway manipulation.

I would like to thank all the graduate students from Garcia Polymer Center for their friendship and support. I could not have achieved this without all your help.

Finally I want to dedicate my love and thanks to my family back in China for all their love and encouragement for my entire life.

Publications

1. Qin S, Clark RAF, Rafailovich MH, The Correlations in En-mass Migration of Adult Human Dermal Fibroblasts on Oriented Fibrillar Scaffolds, Biomaterials, 2014. (Submitted)
2. Sisi Qin, Vincent Ricotta, Marcia Simon, Richard AF. Clark, Miriam H. Rafailovich, Continual Cell Deformation Induced via Attachment to Oriented Fibers Enhances Fibroblast Cell Migration, Plos One, 2014. (Submitted)
3. Sisi Qin, Miriam H. Rafailovich, Marcia Simon, Yupo Ma, Jerell Aguila, In vitro expansion of hematopoietic stem cells on gelatin hydrogels, Blood, 2014. (Submitted)

Chapter 1 Introduction

1.1 Biomaterials

A biomaterial is any matter, surface, or construct that interacts with biological systems. As a science, the biomaterials research has been developed for about fifty years, and has experienced steady and strong growth over its history [1-4]. Biomaterials sciences consists the knowledge of medicine, chemistry, biology, materials sciences and engineering (Figure 1.1).

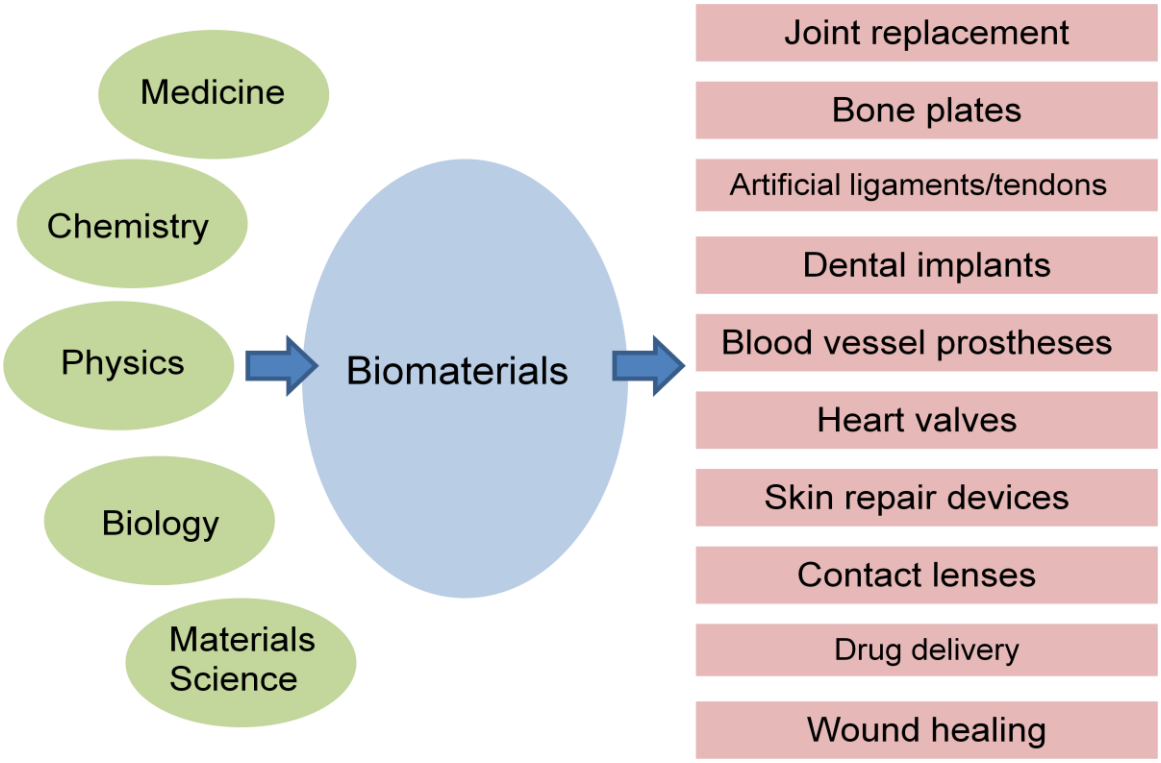

Figure 1.1 Illustration of the interdisciplinary study of biomaterials and their application.

It involves the study of the composition and properties of different materials and the interactions with their environment. Biomaterials are usually integrated into devices and implants other than presence on their own [5-11]. Although biomaterials are primarily used in medical applications, they have also been widely seen in the usage of cell growth, clinical laboratory blood test, biotechnology, biosensors and biochips [12-16]. Biomaterials have been an exciting and novel field for scientists, and the application of the technology is limitless.

The study of biomaterials has some unique characterizations compared to other science. For example, it's a very interdisciplinary science including the study of bioengineering, chemistry, electrical engineering, mechanical engineering, materials sciences, biology, microbiology, and physics. In some occasions, researchers also have to consider the ethics, regulations, and economy issues involved in the study. Secondly, the variety of materials can be used is diversified, where it could be synthetic such as polymers and metals, and it could also made from natural materials or a combination of the two. Finally, the end product of this science is the development of devices. Biomaterials need to be fabricated into devices in order to make a useful clinical therapy [17].

This dissertation focused on the fabrication of polymeric biomaterials of electrospun fibers and synthesized hydrogel, their enhancement of cell function, and the possible applications in the fast wound healing and *in vitro* expansion of hematopoietic stem cells. It showed that substrates topography and mechanics play an important role in cell migration, cell proliferation and cell differentiation.

1.2 Wound healing

One of the most common applications of biomaterials is to address fast wound healing via quick delivery of fibroblasts into the wound. Fibroblast is one of the most important cell types in wound healing since it's responsible for laying down the proper extra cellular matrix (ECM) and collagen in order for other cells to migrate into the wound [18-21]. The wound healing process consists with three major steps: inflammation, granulation tissue formation and scar constitution [22-24]. The fibroblasts activation and migration is the time-limiting steps in granulation tissue formation [25]. First, the wounded area forms fibrin clots together with the re-epithelialization which occurs within minutes and hours. At day 4-6, the granulation tissue begins to form and finally, the wound starts to remodel which takes place around day 7-10.

Various cell types are involved in the migration of the wound. One category of cells is the "fibroblast-like" cells such as pre-adipotye and fibroblasts, where they prefer to reduce crowding and cell-cell contact and migrate individually. The "colony-forming" cells, including endothelial cells and keratinocytes, rather maintain attachment in order to survive. The migration mechanism is expected to be very different for different types of cells. In this study, I focused on the cell migration study on fibroblasts.

1.3 Fibroblast cell migration

The classic mechanism of fibroblast cell migration consists of three steps: extension, attachment, and contraction. The whole process repeats itself so that the cell is able to move forward. First, when the cell senses a signal, it becomes polarized and extends its protrusion at the front end. Second, integrins, which are normally free of cytoskeletal attachments, attach to the retrograde-moving actin filaments after binding to ligand presented on the substrate. And then, cells contract from the rare ends in towards the nucleus while releasing attachment from the receptor accompanied, resulting a translocation of the cell. There are two major mechanisms of release: (i) a mechanical release and (ii) enzymatic release. Recycling of the above process is continuous and cell migration is in progress [26-28].

1.4 Factors affecting cell migration

Different Extracellular Matrix (ECM) environment provides with different chemical or mechanical cues and hence affect cell behaviors [29-31]. Varies factors are included during cell migration such as: growth factor, integrins, and substrate properties [Figure 1.2].

Growth factor: Cell migration starts with a signaling of growth factor that directs cell extension and protrusion. With patterned growth factor, cells are capable to migration under certain guidance. The amount of growth factor can also affect the cell dynamics such as cell migration velocity on the ECM [32].

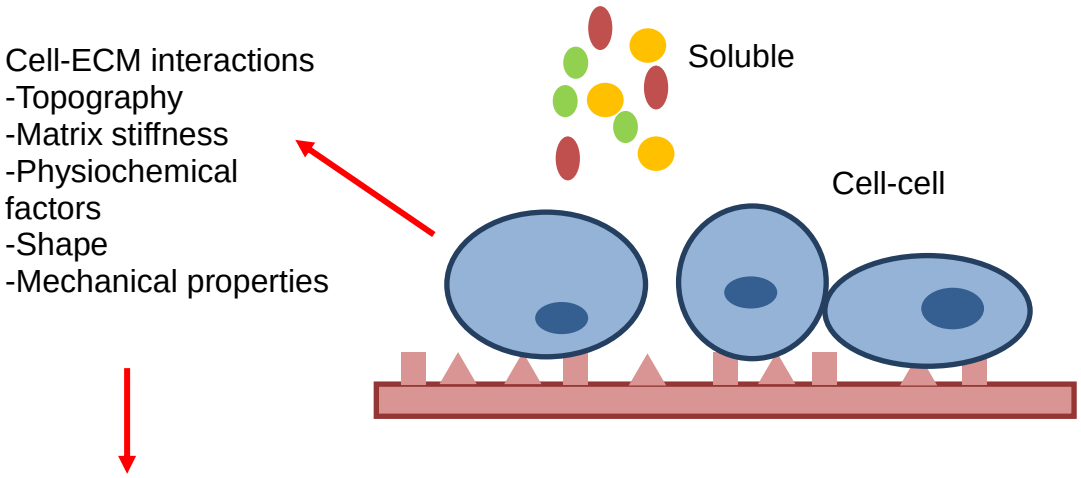

Figure 1.2 Illustration of cell-ECM interactions.

Proteins: Cells can bind to the proteins in the extracellular matrix and interact with it. Important proteins including fibronectin, laminin and collagen can interact with the cells in multiple ways and change cell migration behaviors. Proteins inside the cells such as vinculin, paxillin, F-actin, myosin, and microtubules can also alter fibroblast cell functions and change cell adhesions, cell proliferations and cell migration [33-40].

One of the most important proteins in fibroblast cell migration – fibronectin can binds to ECM macromolecules and facilitates their binding to transmembrane integrins. The attachment of fibronectin to the extracellular domain initiates intracellular signaling pathways as well as association with the cellular cytoskeleton via a set of adaptor molecules such as actin [40].

Substrate properties: Substrate mechanics can affect cell dynamics in many ways. For example, the rigidity of substrate can determine cell morphology and

dynamics. It has been reported that decrease rigidity of substratum is associated with enhanced cellular motility [41]. Another important affect results from the substrate topology. Jeon et al. found that with different topology or pattern of substrate, cell migration motility, migration angle, and migration speed could be changed [42]. The cell migration behavior is very different for cells interacting with flat, nano-size and micron-size substrates [Figure1.3].

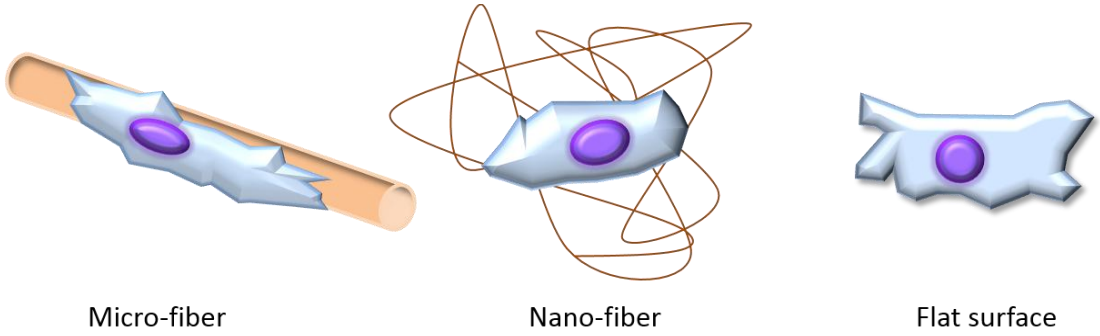

Figure 1.3 Illustration of cell interact with different sizes of ECM fibers.

Since *in vivo*, cell migration occurs along fibers, not flat surfaces, therefore it is important to have models of cell motion on fibers in order to understand the process *in vivo*. Also, since there are multiple fiber sizes, depending on the tissue and process in the real ECM, it is critical to find out how cells behave on different sizes of fibers and to understand what fiber structure is more effective.

The objectives of this research are to:

(1) Fabricate a proper scaffold structure that assist in quick delivery of cells into the wound and aim at fast wound healing.

(2) Study the interactions between fibrillar substrates and the cell migration behavior which in return provide fundamental understanding in the wound healing.

(3) Explore the role of important factors associate with cell migration including focal adhesion, nucleus, and cytoskeleton.

1.5 Bone marrow hematopoietic stem cell

Stem cells are the special cells that possess the capability to differentiate into other different cells types in the body. Also, in many tissues, they can serve as internal repair systems [43, 44]. When a stem cell divides, it can remain as a stem cell or becomes more specialized cell. The stem cell therapy is very important since it has a great potential in treating various disease such as spinal cord injury, burns, heart disease, and bone marrow transplantation. However, the number of people needing a transplant nowadays far exceeds the number of organs available for transplantation, so it will be a tremendous break through if these cells can be cultured in-vitro, and still be able to transplant back into human body without causing long-term problems.

The bone marrow is one of the richest sources of adult stem cells, and the bone marrow hematopoietic stem cells (HSCs) are considered as “non-adherent” cells [45, 46], as oppose to fibroblasts, which can generate strong interactions with the substrate and sense the properties of underlying surface. However, we want to study whether HSCs sense polymeric substrates and change behaviors accordingly.

Most of the stem cell researches nowadays only focus on how to differentiate stem cells into different types of special cells [47-50] as shown in figure 1.4. However, in this research, I aim at the pluripotency preservation of stem cells for bone marrow transplantations, and for the optimum usage of stem cell, it is crucial to maximize its proliferation and minimize its differentiation during cell culture. The current culturing method is usually accomplished in-vivo, which costs a great deal of trouble, so I investigated whether the HSCs can be directly cultured on polymeric substrates, in the absence of additional factors.

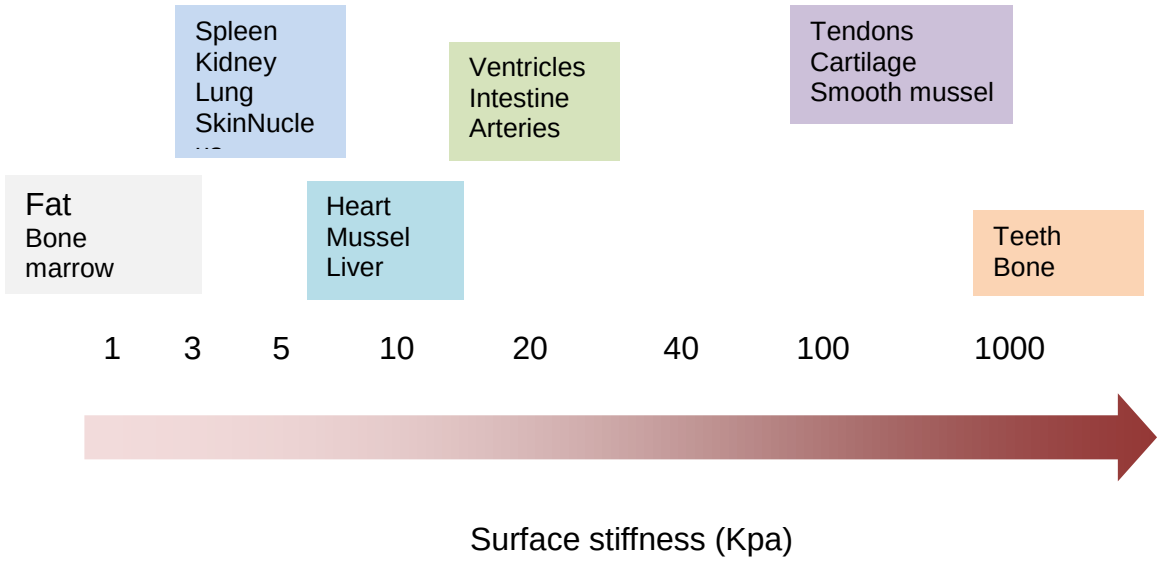

Figure 1.4 Stem cell differentiations on different stiffness surfaces.

1.6 References

[1] Holzapfel BM, Reichert JC, Schantz JT, Gbureck U, Rackwitz L, Nöth U, Jakob F, Rudert M, Groll J, Hutmacher DW, How smart do biomaterials need to be? A translational science and clinical point of view, Adv Drug Deliv Rev, 2013, 65:581-603.

[2] Suh H, Recent advances in biomaterials, Yonsei Med J, 1998, 39:87-96.

[3] Williams DF, Biomaterials and biocompatibility, Med Prog Technol, 1976, 20:31-42.

[4] Chen QZ, Harding SE, Ali NN, Lyonn AR, Boccaccini AR, Biomaterials in cardiac tissue engineering: Ten years of research survey, Mater. Sci. Eng. R-Rep, 2008, 59:1-37.

[5] Pérez RA, Won JE, Knowles JC, Kim HW, Naturally and synthetic smart composite biomaterials for tissue regeneration, Adv Drug Deliv Rev, 2013, 65:471-496.

[6] Cen L, Liu W, Cui L, Zhang W, Cao Y, Collagen tissue engineering: development of novel biomaterials and applications, Pediatr Res, 2008, 63:492-496.

[7] Hallab N, Link HD, McAfee PC, Biomaterial optimization in total disc arthroplasty, Spine (Phila Pa 1976), 2003, 28:S139-152.

[8] Franz S, Rammelt S, Scharnweber D, Simon JC, Immune responses to implants - a review of the implications for the design of immunomodulatory biomaterials, Biomaterials, 2011, 32:6692-6709.

[9] Barrèrea F, Mahmoodb TA, de Groota K, van Blitterswijk CA, Advanced biomaterials for skeletal tissue regeneration: Instructive and smart functions, Mater. Sci. Eng. R-Rep, 2008, 59, 38-71.

[10] Chen QZ, Liang SL, Thouas GA, Elastomeric biomaterials for tissue engineering, Prog. Polym. Sci, 2013, 38:584-671.

[11] Gosain AK, Persing JA, Biomaterials in the face: benefits and risks, J Craniofac Surg, 1999, 10:404-414.

[12] Naderi H, Matin MM, Bahrami AR, Review paper: critical issues in tissue engineering: biomaterials, cell sources, angiogenesis, and drug delivery systems, J Biomater Appl, 2011, 26:383-417.

[13] Waite JH, Broomell CC, Changing environments and structure--property relationships in marine biomaterials, J Exp Biol, 2012, 215(Pt 6):873-883.

[14] Liu XY, Chu PK, Ding CX, Surface nano-functionalization of biomaterials, Mater. Sci. Eng. R-Rep, 2010, 70:275-302.

[15] Shao Y, Fu JP, Integrated Micro/Nanoengineered Functional Biomaterials for Cell Mechanics and Mechanobiology: A Materials Perspective, Adv. Mater, 2014, 26: 1494-1533.

[16] Rahmany MB, Van Dyke M, Biomimetic approaches to modulate cellular adhesion in biomaterials: A review, Acta Biomater, 2013, 9:5431-5437.

[17] Langer R, Tirrell DA, Designing materials for biology and medicine, Nature, 2004, 428:487-492.

[18] Bainbridge P, Wound healing and the role of fibroblasts, J Wound Care. 2013, 22:407-8, 410-12.

[19] Boateng JS, Matthews KH, Stevens HN, Eccleston GM, Wound healing dressings and drug delivery systems: a review, J Pharm Sci, 2008, 97:2892-2923.

[20] Ehrlich HP, Wound closure: evidence of cooperation between fibroblasts and collagen matrix, Eye (Lond), 1988, 2:149-157.

[21] Reinke, JM, Sorg H, Wound Repair and Regeneration, Eur Surg Res, 2012, 49:35-43.

[22] Velnar T, Bailey T, Smrkolj V, The wound healing process: an overview of the cellular and molecular mechanisms, J Int Med Res, 2009, 37:1528-1542.

[23] DiPietro LA, Wound healing: the role of the macrophage and other immune cells, Shock, 1995, 4:233-240.

[24] Diegelmann RF, Evans MC, Wound healing: an overview of acute, fibrotic and delayed healing, Front Biosci, 2004, 9:283-289.

[25] Singer AJ, Clark RAF, A Cutaneous Wound Five Days after Injury, The NEJM, 1999, 341: 738-746.

[26] Kumar V, Fausto N, Abbas A, Pathologic Basis of Disease (7th Edition), 14-16.

[27] Alberts B, Bray D, Hopin K, Johnson A, Lewis J, Raff M, Roberts K, Walter P, Tissues and Cancer, Essential cell biology, 2004:1-38.

[28] Straus AH, Carter WG, Wayner EA, Hakomori S, Mechanism of fibronectin-mediated cell migration: dependence or independence of cell migration susceptibility on RGDS-directed receptor (integrin), Exp. Cell. Res, 1989, 183:126-139.

[29] Newby AC, Matrix metalloproteinases regulate migration, proliferation, and death of vascular smooth muscle cells by degrading matrix and non-matrix substrates, Cardiovasc Res, 2006, 69:614-624.

[30] da Rocha-Azevedo B, Grinnell F, Fibroblast morphogenesis on 3D collagen matrices: the balance between cell clustering and cell migration, Exp Cell Res, 2013, 319:2440-2446.

[31] Kim HD, Peyton SR, Bio-inspired materials for parsing matrix physicochemical control of cell migration: a review, Integr Biol (Camb), 2012, 4:37-52.

[32] Alberts B, Bray D, Hopkin K, Johnson A, Lewis J, Essential cell biology, 2nd Ed.

[33] Horiba K, Fukuda Y, Synchronous appearance of fibronectin, integrin alpha 5 beta 1, vinculin and actin in epithelial cells and fibroblasts during rat tracheal wound healing, Virchows Arch, 1994, 425:425-434.

[34] Pankov R, Cukierman E, Katz BZ, Matsumoto K, Lin DC, Lin S, Hahn C, Yamada KM, Integrin dynamics and matrix assembly: tensin-dependent translocation of alpha(5)beta(1) integrins promotes early fibronectin fibrillogenesis, J Cell Biol, 2000, 148:1075-1090.

[35] Mao Y, Schwarzbauer JE, Accessibility to the fibronectin synergy site in a 3D matrix regulates engagement of alpha5beta1 versus alphavbeta3 integrin receptors, Cell Commun Adhes, 2006, 13:267-277.

[36] Hsia HC, Nair MR, Corbett SA, The fate of internalized α5 integrin is regulated by matrix-capable fibronectin, J Surg Res, 2014, 191:268-279.

[37] Zhang Z, Morla AO, Vuori K, Bauer JS, Juliano RL, Ruoslahti E, The alpha v beta 1 integrin functions as a fibronectin receptor but does not support fibronectin matrix assembly and cell migration on fibronectin, J Cell Biol, 1993, 122:235-242.

[38] Hocking DC, Sottile J, Langenbach KJ, Stimulation of integrin-mediated cell contractility by fibronectin polymerization, J Biol Chem, 2000, 275:10673-10682.

[39] Huveneers S, Truong H, Fässler R, Sonnenberg A, Danen EH, Binding of soluble fibronectin to integrin alpha5 beta1 - link to focal adhesion redistribution and contractile shape, J Cell Sci, 2008, 121(Pt 15):2452-2462.

[40] Alberts B, Bray D, Hopin K, Johnson A, Lewis J, Raff M, Roberts K, Walter P Tissues and Cancer, Essential cell biology, 2004.

[41] Schindler M, Nur-E-Kamal A, Ahmed L, Kamal J, Liu HY, Amor N, Ponery AS, Crockett DP, Grafe TH, Chung HY, Weik T, Jones E, Meiners S, Living in Three Dimensions-3D Nanostructured Environments for Cell Culture and Regenerative Medicine, Cell Biochem Biophys, 2006, 45:215-227.

[42] Jeon H, Hidai H, Hwang DJ, Healy KE, Grigoropoulos CP, The effect of micronscale anisotropic cross patterns on fibroblast migration, Biomaterials, 2010, 31:L4286–4295.

[43] Ho PJ, Yen ML, Yet SF, Yen BL, Current applications of human pluripotent stem cells: possibilities and challenges, Cell Transplant, 2012, 21:801-814.

[44] Tao H, Ma DD, Evidence for transdifferentiation of human bone marrow-derived stem cells: recent progress and controversies, Pathology, 2003, 35:6-13.

[45] Wlodarski KH, Galus R, Wlodarski P, Non-adherent bone marrow cells are a rich source of cells forming bone in vivo. Folia Biol (Praha), 2004 50: 167–173.

[46] Clarke E, McCann SR, Stromal colonies can be grown from the non-adherent cells in human long-term bone marrow cultures. Eur J Haematol, 1991, 46: 296–300.

[47] Leipzig ND, Shoichet MS, The effect of substrate stiffness on adult neural stem cell behavior, Biomaterials, 2009, 30:6867-6878.

[48] Nam J, Johnson J, Lannutti JJ, Agarwal S, Modulation of embryonic mesenchymal progenitor cell differentiation via control over pure mechanical modulus in electrospun nanofibers, Acta Biomater, 2011, 7:1516-1524.

[49] Hazeltine LB, Badur MG1, Lian X, Das A, Han W, Palecek SP, Temporal impact of substrate mechanics on differentiation of human embryonic stem cells to cardiomyocytes, Acta Biomater, 2014, 10:604-612.

[50] Hu X, Park SH, Gil ES, Xia XX, Weiss AS, Kaplan DL, The influence of elasticity and surface roughness on myogenic and osteogenic-differentiation of cells on silk-elastin biomaterials, Biomaterials, 2011, 32:8979-8989.

Chapter 2 Experimental techniques

2.1 Spin-casting

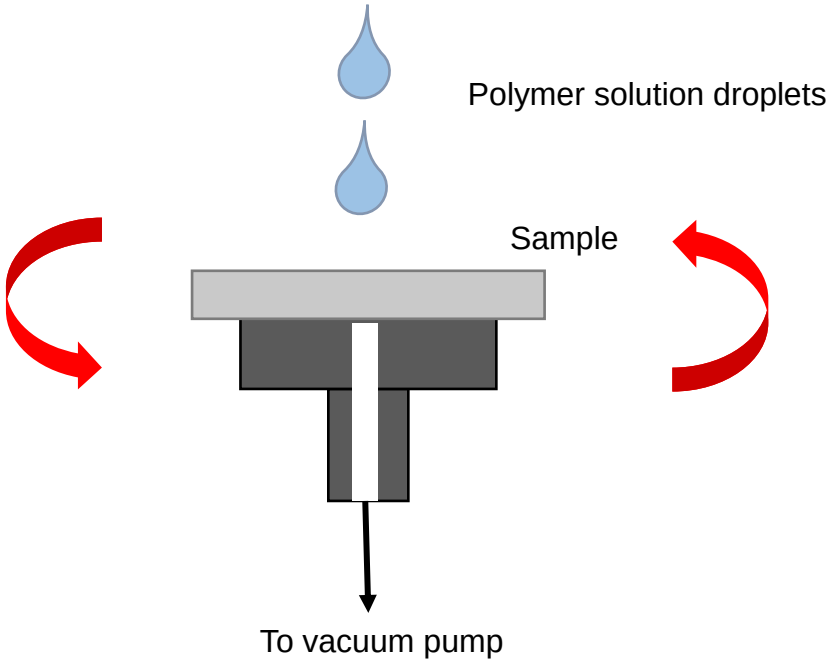

Figure 2.1 Diagram of spin-casting.

Spin casting offers a rapid, reliable method of depositing thin films from solution. It produces films in which molecular order is non-controllable (and in fact, usually produces disordered films) [1]. This method is widely employed in industry for deposition of photoresists, and more recently, active layers in organic light emitting diodes.

A few drops of solution are placed on to the surface of the substrate. The amount of solution and rate of dropping, have little effect on the final film properties (Figure 2.1).

The substrate is rotated at several thousand rpm. Film thickness is determined by the spinning speed (faster speeds result in thinner films) and the solution viscosity (lower viscosity gives thinner films) [2, 3]. Scientists have been studying the factors

influencing the final thin film thickness and structure such as solution concentration, humidity, polymer properties, and glass transition, with various polymers [4-10].

2. 2 Electrospinning

Electrospinning is a crucial technique in this research. It transforms liquid polymer solutions into submicron-scale fibers, and provides special properties that are desired in the experiment.

Polymers must be well dissolved before electrospinning, and a homogeneous solvent is crucial for making uniform fibers. The polymer fluid is then introduced into spinneret. After that, a high voltage electric field is applied to the tip of the spinneret, and counteracts with the surface tension of the solvent within. When it reaches a certain point, the repulsive electrical force overcomes the surface tension, and a charged jet of solution will be ejected from the tip of needle. After the solvent evaporated, desired polymer fibers will be left on the grounded collector (Figure 2.2). Since polymer trains are usually entangled with each other, it is possible to form a long enough polymer fibers and the whole process is continuous.

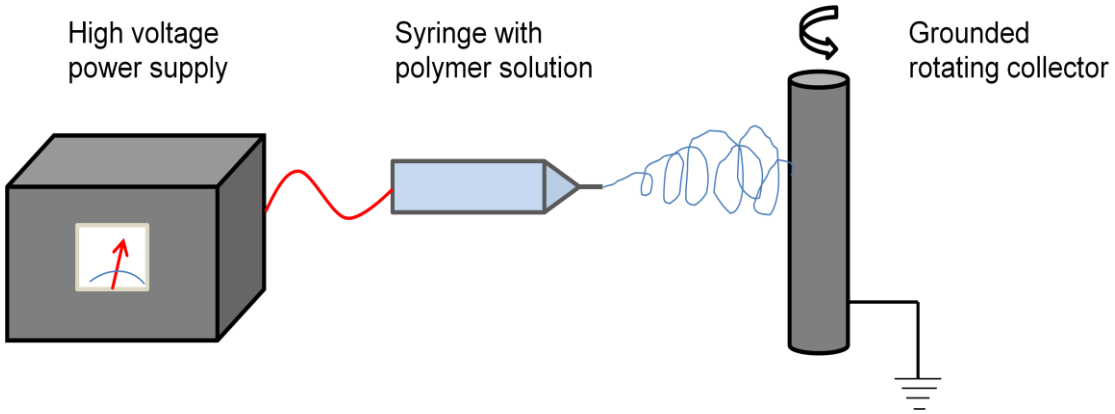

Figure 2.2 Set up of electrospinning.

2. 3 AFM

Atomic force microscopy (AFM) or scanning force microscopy (SFM) is a very high-resolution type of scanning probe microscopy, with demonstrated resolution on the order of fractions of a nanometer, more than 1000 times better than the optical diffraction limit. The AFM is one of the foremost tools for imaging, measuring, and manipulating matter at the nanoscale. The information is gathered by "feeling" the surface with a mechanical probe. Piezoelectric elements that facilitate tiny but accurate and precise movements on (electronic) command enable the very precise scanning [11].

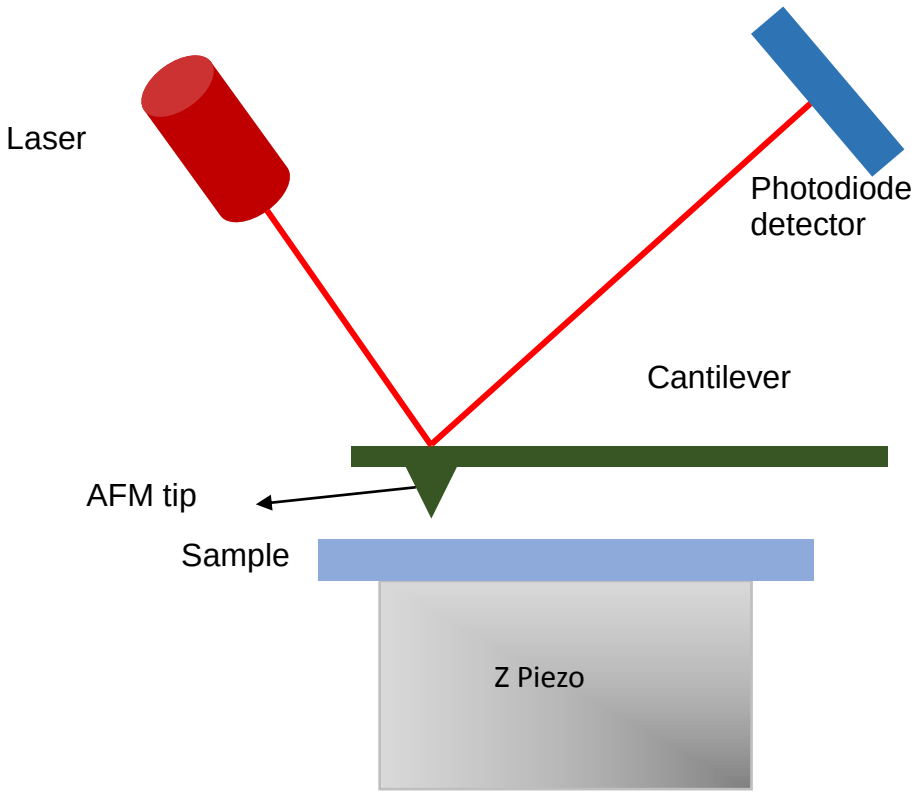

Figure 2.3 Illustration of AFM.

AFM has found itself a prominent future in the study of polymer thin films and biological performance of live cells [12, 13]. It has been widely used in the study of cell membranes, cell mechanics, biosensors, microbiology, cancerology, and also the intermolecular interactions and cell surface morphology [14-21].

In this research, a Dimension 3000 (Digital Instruments, Santa Barbara, CA) shear modulation force microscopy is used which also equipped with a standard 100 *í*mXY and 10 *í*mZ piezo scanner. As simply illustrated in Figure 2.3, a sinusoidal drive signal is applied to the *X*-piezo with a frequency of 1400 Hz, resulting a small oscillatory

motion of the AFM tip. The tip is laterally modulated and its response is recorded by a dual phase lock-in amplifier. When measuring the sample, a normal force of 25 nN is applied to the tip in order to maintain the contact between surface and the tip. The response amplitude (mV) of the cantilever is measured and be plotted against the drive amplitude (mV), giving a proportional reading.

2. 4 Confocal microscopy

Confocal microscopy is an optical imaging technique used to increase optical resolution and contrast of a micrograph by using point illumination and a spatial pinhole to eliminate out-of-focus light in specimens that are thicker than the focal plane (Figure 2.4). It enables the reconstruction of three-dimensional structures from the obtained images. This technique has gained popularity in the scientific and industrial communities and typical applications are in life sciences, semiconductor inspection and material science [22-24].

By using confocal microscope, the morphology of cells on different planes can be clearly detected, and with multiple layers scanning, a 3-D image of cells can be taken and gives people a better understanding of cell morphology in three dimension matrix [25-28].

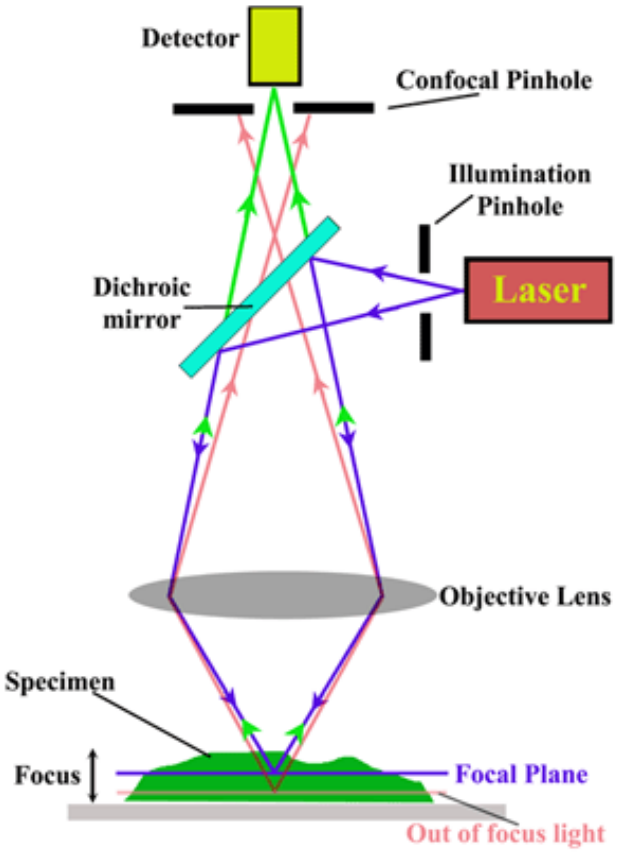

Figure 2.4 Layout of confocal microscopy.

2. 5 MetaMorph®-operated CoolSNAP™HQ camera attached to a Nikon Diaphot-TMD inverted microscope

Fluorescent dyes used for staining cells are detected with the aid of fluorescence microscope. This microscope is similar to an ordinary light microscope except that the illuminating light is passed through two sets of filter. The first filters the light before it

reaches the specimen, passing only those wavelengths that excite the particular fluorescent dye. The second blocks out this light and passes only those wavelengths emitted when the dye fluoresces. Dyed objects show up in bright color on a dark background [29].

Metamorph imaging system can be used to acquire pictures over time and edited into a movie. It is also capable in the field of morphometric study, region measurement, multi-dimensional imaging, and distance analyzing. This time-lapse imaging is a very powerful tool in cell dynamics study [30-33].

2.6 Flow cytometer

Flow cytometry is a commonly used technology that can measure and analyze multiple physical and chemical characteristics of single particles simultaneously for up to thousands particles per second. It has been widely applied in biology studies and medical analysis when cells are suspended in a flow steam of fluid and detected and analyzed by an electronic detection apparatus [34]. Flow cytometer is routinely used in cell counting, cell sorting, biomarker detection, protein engineering and in the diagnosis of health disorders, especially blood cancers [35-38]. After the flow cytometer measurements, the particle's relative size, relative granularity or internal complexity, and relative fluorescence intensity can be identified.

A flow cytometer is usually made up of three main systems: fluidics, optics, and electronics. As shown in Figure 2.5, the fluidics system is aimed to transport particles (commonly cells in biological use) in a stream of fluid to the laser beam for further

detection. Particles are focused as single particle when go through the fluidics system when they are confined by hydrodynamic focusing.

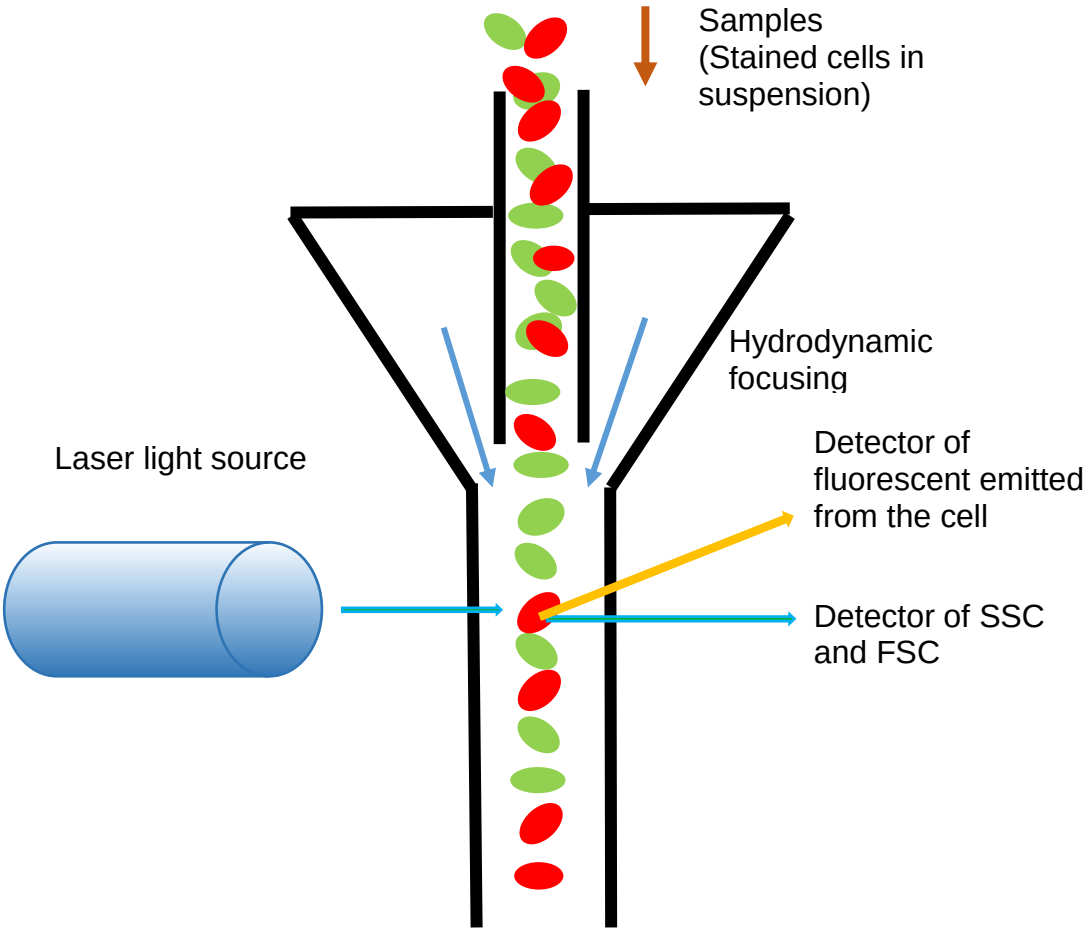

Figure 2.5 Illustration of flow cytometer.

There are two parts in the optical system, where one is the excitation optics and the other is the collection optics. The excitation optics includes the laser and lenses which can be used to shape and focus the laser beam. The collections optics has a collection lens to collect the emitted lights, and a system of optical mirrors and filters. Two types of light scattering occur when particle interacts with the light. Side-scattered light (SSC) is proportional to cell granularity or internal complexity and is usually

collected at approximately 90 degrees to the laser beam, while Forward-scattered light (FSC) is proportional to cell-surface area or size. Fluorescence labeled particles can also be detected by the flow cytometer. When a fluorescent dye is conjugated to an antibody, it can be used to identify a particular character of a cell based on the antigenic surface markers [39].

The above techniques had been fully applied in the study of biomaterials and the biological system that they encountered. The detailed procedure of each equipment will be further discussed in each chapter.

2.7 References

[1] Frank CW, Rao MM, Pease RFW, Hinsberg WD, Miller RD, Rabolt JF, Structure in Thin and Ultrathin Spin-Cast Polymer Films, Science, 1996, 273: 912-915.

[2] Walheim S, Boltau M, Mlynek J, Krausch G, Steiner U, Structure formation via polymer demixing in spin-cast films, Macromolecules 1997, 30: 4995–5003.

[3] Bernasik A, Wlodarczyk-Miœkiewicz J, Luzny W, Kowalski K, Raczkowska J, Rysz J, Budkowski A, Lamellar structures formed in spin-cast blends of insulating and conducting polymers. Synth. Met, 2004, 144: 253–257.

[4] Richardson H, López-García I, Sferrazza M, Keddie JL, Thickness dependence of structural relaxation in spin-cast, glassy polymer thin films, Phys. Rev, 2004, 70:e051805.

[5] Sanat KE, Kumar SK, Douglas JF, Karim A, The Critical Role of Solvent Evaporation on the Roughness of Spin-Cast Polymer Films, Macromolecules, 2001, 34: 4669–4672.

[6] Myers JN, Zhang C, Chen C, Chen Z, Influence of casting solvent on phenyl ordering at the surface of spin cast polymer thin films, J Colloid Interface Sci, 2014 , 423:60-66.

[7] Dunbar AD, Mokarian-Tabari P, Parnell AJ, Martin SJ, Skoda MW, Jones RA, A solution concentration dependent transition from self-stratification to lateral phase separation in spin-cast PS:d-PMMA thin films, Eur Phys J E Soft Matter, 2010, 31:369-75.

[8] Madej W, Budkowski A, Raczkowska J, Rysz J, Breath figures in polymer and polymer blend films spin-coated in dry and humid ambience, Langmuir, 2008, 24:3517-3524.

[9] Richardson H, López-García I, Sferrazza M, Keddie JL, Thickness dependence of structural relaxation in spin-cast, glassy polymer thin films, Phys Rev E Stat Nonlin Soft Matter Phys, 2004, 70(5 Pt 1):051805.

[10] Richardson H, Sferrazza M, Keddie JL, Influence of the glass transition on solvent loss from spin-cast glassy polymer thin films, Eur Phys J E Soft Matter, 2003, 12 Suppl 1:S87-91.

[11] Giessibl FJ, Advances in atomic force microscopy, Reviews of Modern Physics, 2003, 75:949.

[12] Passeri D, Rossi M, Tamburri E, Terranova ML, Mechanical characterization of polymeric thin films by atomic force microscopy based techniques, Anal Bioanal Chem, 2013, 405:1463-1478.

[13] Morkvėnaitė-Vilkončienė I, Ramanavičienė A, Ramanavičius A, Atomic force microscopy as a tool for the investigation of living cells. Medicina (Kaunas), 2013, 49:155-164.

[14] Whited AM, Park PS, Atomic force microscopy: a multifaceted tool to study membrane proteins and their interactions with ligands. Biochim Biophys Acta, 2014, 1838(1 Pt A):56-68.

[15] Pillet F, Chopinet L, Formosa C, Dague E, Atomic Force Microscopy and pharmacology: from microbiology to cancerology, Biochim Biophys Acta, 2014, 1840:1028-1050.

[16] Benitez R, Toca-Herrera JL, Looking at cell mechanics with atomic force microscopy: Experiment and theory, Microsc Res Tech**,** 2014, doi: 10.1002/jemt.22419.

[17] Vahabi S, Nazemi Salman B, Javanmard A, Atomic force microscopy application in biological research: a review study, Iran J Med Sci, 2013, 38:76-83.

[18] Steffens C, Leite FL, Bueno CC, Manzoli A, Herrmann PS, Atomic force microscopy as a tool applied to nano/biosensors, Sensors (Basel), 2012,12:8278-8300.

[19] Dorobantu LS, Goss GG, Burrell RE, Atomic force microscopy: a nanoscopic view of microbial cell surfaces, Micron, 2012, 43:1312-1322.

[20] Picas L, Milhiet PE, Hernández-Borrell J, Atomic force microscopy: a versatile tool to probe the physical and chemical properties of supported membranes at the nanoscale, Chem Phys Lipids, 2012, 165:845-860.

[21] Safenkova IV, Zherdev AV, Dzantievf BB, Application of atomic force microscopy for characteristics of single intermolecular interactions, Biochemistry (Mosc), 2012, 77:1536-1552.

[22] Pawley JB, Handbook of Biological Confocal Microscopy (3rd Edition), 2006.

[23] Nwaneshiudu A, Kuschal C, Sakamoto FH, Anderson RR, Schwarzenberger K, Young RC, Introduction to confocal microscopy, J Invest Dermatol. 2012, 132:e3.

[24] White J, Reflecting on confocal microscopy: a personal perspective, Methods Mol Biol, 2014, 1075:1-7.

[25] Patel DV, McGhee CN, Quantitative analysis of in vivo confocal microscopy images: a review,Surv Ophthalmol, 2013, 58:466-475.

[26] Jensen E, Technical review: colocalization of antibodies using confocal microscopy, Anat Rec (Hoboken), 2014, 297:183-187.

[27] Martinez-Santibañez G, Cho KW, Lumeng CN, Imaging white adipose tissue with confocal microscopy, Methods Enzymol, 2014;537:17-30.

[28] Zhang LW, Monteiro-Riviere NA, Use of confocal microscopy for nanoparticle drug delivery through skin, J Biomed Opt, 2013, 18:061214.

[29] Bruce Alberts, Dennis Bray, Karen Hopkin, Alexander Johnson, Julian Lewis, Essential cell biology (2nd Edition), 2009.

[30] Funahashi J, Nakamura H, Time-lapse imaging system with shell-less culture chamber, Dev Growth Differ, 2014, 56:305-309.

[31] Golchin SA, Stratford J, Curry RJ, McFadden J, A microfluidic system for long-term time-lapse microscopy studies of mycobacteria, Tuberculosis (Edinb), 2012, 92:489-496.

[32] Snapp EL, Lajoie P.Time-lapse imaging of membrane traffic in living cells, Cold Spring Harb Protoc, 2011, 11:1362-1365.

[33] Khlghatyan J, Saghatelyan A, Time-lapse imaging of neuroblast migration in acute slices of the adult mouse forebrain, J Vis Exp, 2012, 67:e4061.

[34] Pedreira CE, Costa ES, Lecrevisse Q, van Dongen JJ, Orfao A; EuroFlow Consortium, Overview of clinical flow cytometry data analysis: recent advances and future challenges, Trends Biotechnol, 2013, 31:415-425.

[35] Reardon AJ, Elliott JA, McGann LE, Fluorescence as an alternative to light-scatter gating strategies to identify frozen-thawed cells with flow cytometry, Cryobiology, 2014, 69:91-99.

[36] Krause DS, Delelys ME, Preffer FI, Flow cytometry for hematopoietic cells, Methods Mol Biol, 2014, 1109:23-46.

[37] Rundberg Nilsson A, Bryder D, Pronk CJ, Frequency determination of rare populations by flow cytometry: a hematopoietic stem cell perspective, Cytometry A, 2013, 83:721-727.

[38] Juan-García A, Manyes L, Ruiz MJ, Font G, Applications of flow cytometry to toxicological mycotoxin effects in cultured mammalian cells: a review, Food Chem Toxicol, 2013, 56:40-59.

[39] Rahman M, Introduction to Flow Cytometry, AbD Serotec, 2014.

Chapter 3 The role of oriented fibrillar scaffods in establishing correlations in the en-mass migration of dermal fibroblasts

3.1 Introduction

It is well-established that in vivo cell migration occurs on fibrillar rather than flat surfaces [1-3] and the migration process is a critical step in the wound healing process [4, 5]. Collective migration where cells migrate together while maintaining cell-cell contacts has been studied extensively [6-10], yet only few studies have been reported regarding en-mass migration [11, 12] or the process preferred by fibroblasts. In this case most studies have focused on the dynamics of isolated cells, which given that cell-cell interactions are also important among fibroblasts, and hence the results on single cells may be different than those obtained from multi-cell studies. For example, Liu et al. [11] compared en-mass migration of fibroblasts out of an agarose droplet to single cell migration onto flat and fibrillar surfaces. On flat surfaces, fibroblasts migrated outward into a “sunburst’ type pattern in a trajectory aimed increasing the separation between adjacent cells while the speed of the cells decreased with increasing distance from the droplet, reaching the single cell migration value after 24 hours. In contrast, cells migrating outward from droplets placed on fibers experienced a “bottleneck” effect, as they emerged en–mass with the single cell velocity which remained unchanged for the first 24 hours. It has also been shown that three dimensional migration of human dermal fibroblasts on a fibrous scaffolds, having diameters one micron or larger, did not proceed via cell migration within the pores of the scaffold [13]. Rather, the migration occurred only along the fibers, where motion from one layer to the next involved a sudden change in trajectory at the junction of fibers in different layers. Hence it appeared that the major factors determining the magnitude and direction of the

migration speed were the nature of the fiber junctions, rather than the porous structure of the scaffold.

It has been shown in several studies that cell migration was affected by the topography of the underlying substrate [14-20], which in turn determined other parameters such as density and distribution of the focal adhesion points [21-25] the degree of nuclear deformation [26-29]. In the case of en-mass migration of cells on scaffolds, the angle between fibers, or the angle at the junction points, can also be element determining the substrate topography. Hence the question arises whether cells could discriminate between junction points having different angles and exhibit a preference for migration in a specific direction.

In order to address these questions, I have devised a technique for producing a multi-layered scaffold where the angle between fibers can be precisely controlled and the influence of the three dimensional substrate morphology on the migration behavior determined. I chose to use the well-established droplet technique [30-32] for studying en-mass migration behavior rather than scratch assays [33-35] since it allows for better quantification of the cell migration trajectories and the behavior of individual cells within the migrating ensemble. The answers to these questions can further our understanding of the elements within the substrate that control outward cell migration and can enhance our ability to engineer structures essential for wound healing applications.

3.2 Materials and Methods

3.2.1 Fabrication of electrospun PMMA scaffolds of variable angle

The application of the multilayered scaffold is preceded by preparation of the substrate with a flat spun cast film. The film allows for adhesion of the scaffold, as well as for a direct comparison between cells on flat vs fibrillar surfaces. Poly (methyl methacrylate) (PMMA) (Mw=120,000 Da, Sigma-Aldrich) was dissolved in toluene ((Fisher Scientific, Pittsburgh, PA) at 30mg/mL, and then spin-casted on 1.5 cm diameter glass cover slips at 2500PRM for 30 seconds.

Electrospun fibers of different diameters were produced by dissolving PMMA in different solvents, as listed in table 3.1, where the solvent and concentrations were optimized to minimize beading and produce fibers of the desired diameters**.**

Concentration of PMMA	Solvent	Results
30%	THF + DMF (1:1)	1μm fibers
30%	DMF + Chloroform(1:1)	4μm fibers
20%	Chloroform	8μm fibers

Table 3.1 Solvent and concentration of PMMA for producing different sizes of electrospun fibers.

The set up for obtaining oriented multi layered scaffolds is illustrated in figure 3.1a. Fiber alignment was accomplished by placing the PMMA coated cover slips on a drum whose diameter, 10 cm, was much larger than that of the cover slips, and which was rotating at a speed of 6750 r/min. The distance between adjacent fibers was controlled by the electrospinning time, where mean distances of 30, 50, and 100μm were achieved with spinning times of 1, 2.5, and 5 min. The angular orientation of the cover slips was marked by fiduciary on the drum as shown. The angle between different layers could then be precisely controlled via rotation of the cover slip after deposition of each layer. The samples were then annealed in a vacuum of 10^{-7} Torr at 120°C overnight to remove the remaining solvent and sterilize the samples.

a

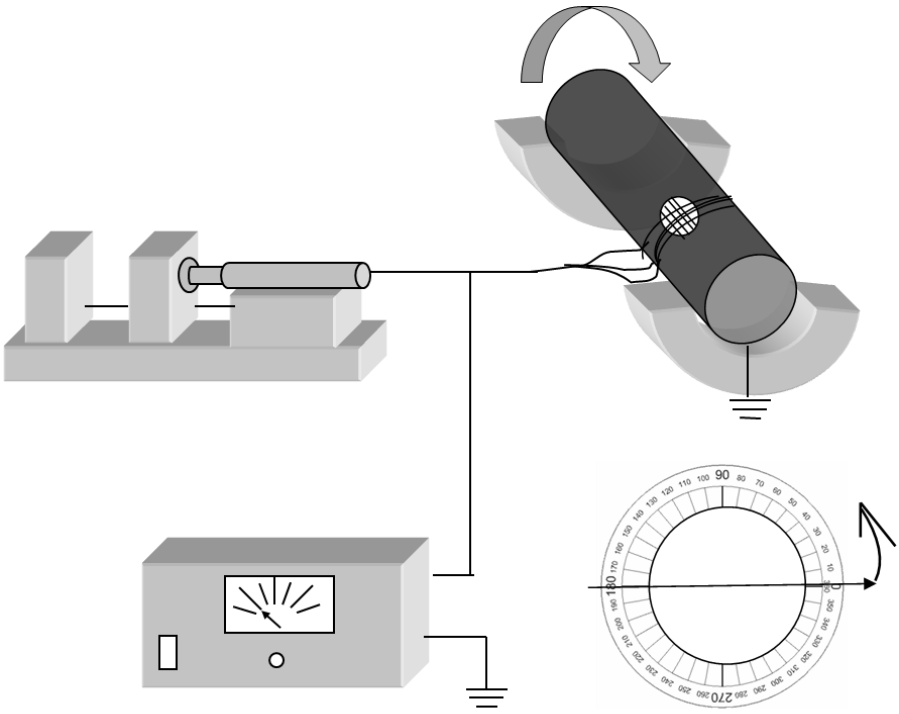

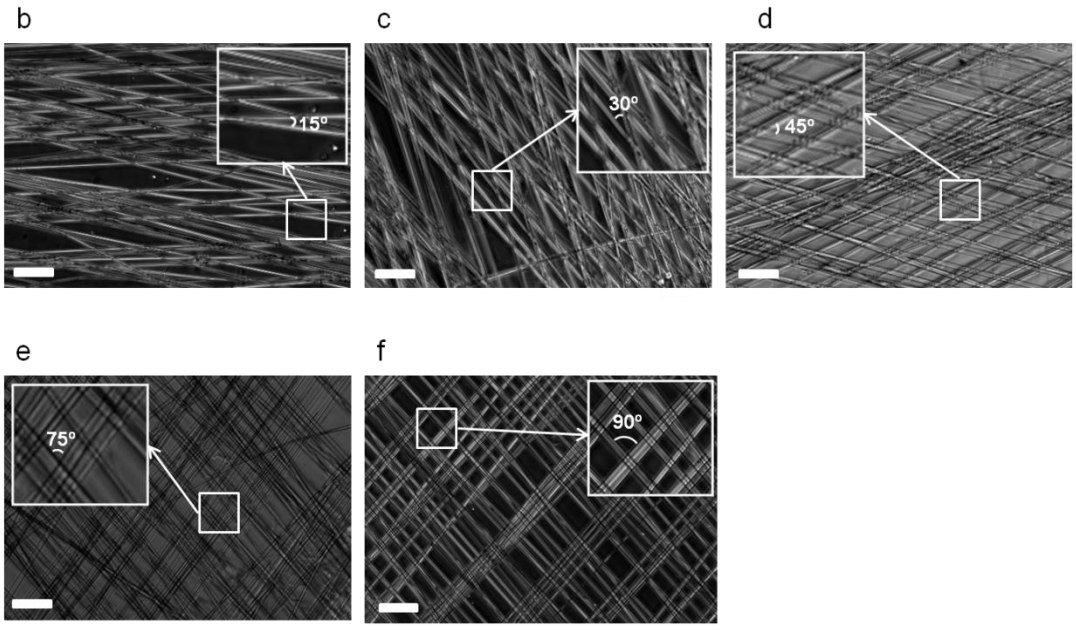

Figure 3.1 Electrospun PMMA scaffolds. (a) Illustration of electrospinning setup for fabricating designed angle scaffolds. (b) 15˚, (c) 30 ˚, (d) 45 ˚, (e) 75 ˚, and (f) 90 ˚ (Scale bar=100 μm).

Figure 3.1b-3.1f shows the phase contrast images of samples with angles of 15˚, 30˚, 45˚, 75˚, and 90˚ between adjacent layers of fibers. From the figure one can see that even though the spacing between fibers has a large variation, the angle between fibers in adjacent layers is uniform. I have previously shown that for an orthogonal scaffold, the spacing between fibers need only be large enough to allow cells attached to fibers to penetrate, and hence did not affect the migration when they were in a range from 10-100 microns. The spacing between the fibers shown in figure 3.1b-3.1f was easily controlled within this range and hence no further processing [36, 37] was applied to try to reduce the variation.

3.2.2 Cell culture

Adult Human Fibroblast Cell (CF29) was purchased from ATCC (Manassas, VA), and cultured in Dulbecco's Modified Eagle Medium (DMEM), together with 10% fetal bovine serum (Hyclone, Logan, UT), 1% antibiotic mix of penicillin, streptomycin, and L-glutamine (GIBCO BRL/Life Technologies, Grand Island, NY), (referred to as full-DMEM), in a humidified incubator at 37°C with 5% CO_2. Before seeding the cells, the samples were further sterilized by exposure to the UV within the BSL-2 enclosure for 20 min, and then coated with 30mg/mL of intact human plasma fibronectin (Calbiochem, San Diego, CA) in serum-free DMEM for 2 hours in the incubator. Sterilization with alcohol was avoided since it pitted the PMMA surfaces.

3.2.3 Cell membrane staining

Fibroblasts cell membranes were live stained with 1, 1′- dioctadecyl-3, 3, 3′, 3′-tetramethylindodicarbocyanine perchlorate (DiD, Invitrogen, Carlsbad, CA). Cells were washed with phosphate buffer saline (PBS), and suspended in the 3.5 μg/ml DiD-serum free DMEM solution at a density of 1×10^6 cells/mL, then incubated at 37°C for 30 min. The suspension tubes were then centrifuged at 1500RPM for 5 min, and the supernatant was removed.

3.2.4 Droplet migration method

After staining the membrane, the fibroblasts were re-suspended in a volume of 0.2% (w/v) agarose solution to obtain a final cell density of 1.5×10^7 cells/ml. Several droplets of the agarose / cell suspension, each 1.25 µL in volume, were seeded onto the substrates, and solidified by placing at 4 °C for 10 min. Full- DMEM, warmed to 37C was then slowly added to the sample in order to avoid displacement.

3.2.5 Measurement of cell migration

After cell seeding, samples were incubated in the humidified incubator, with 5% CO2, at 37°C for 24 hrs. The migration velocity was measured via time lapse photography by placing the samples on a 37 °C incubator stage attached to a Nikon Diaphot-TMD inverted microscope and fitted with a MetaMorph®-operated CoolSNAP™HQ camera (Universal Imaging Corporation, Downingtown, PA). Images were automatically taken every 15 min over the period of one hour, and the migration velocity of the cells was calculated using MetaMorph. Only the cells that were migrating at the leading edge were chosen for the measurement in order to avoid cell-cell interference. In order to determine the location of the moving front relative to the initial droplet position, fluorescent microscope pictures were overlapped by the images of cells incubated for 4 hours, stained with DiD (red) and the cells incubated for 24 hours, fixed, and stained with Alexa-fluor 488 (green).

3.2.6 Immunofluorescent staining

Location of vinculin was visualized by a Leica TCS SP2 laser scanning confocal microscope (Leica Microsystems, Bannockburn, IL). After incubation, cells were fixed with 3.7% formaldehyde for 20 min, permeabilized with 0.4% Triton for 7 min, and blocked with 2% BSA in PBS for 30 min at room temperature. Immunofluorescent staining for vinculin (Sigma, Saint Louis, MO) was performed at a 1:600 dilution for 1 h then incubated with the Oregan Green 488 goat anti-mouse secondary antibody (Invitrogen, Carlsbad, CA) with the same procedure. To observe the nuclei, cells were stained with 4',6-diamiadino-2-phenylindole (DAPI, Sigma-Aldrich, Inc., St. Louis, USA) for 10 min at room temperature, and the results were quantified using Image J software.

3.2.7 Statistical Analysis

Twenty cells were measured in each sample, and 3 replicate samples were prepared for each condition. Each data point then signified an average over at least 60 cells. Statistical analysis was performed using GraphPad5 software to calculate the statistical significance level using Tukey's HSD test.

3.3 Results and discussion

3.3.1 Dependence on fiber diameter

The en-mass migration profile of cells emerging from droplets positioned on fibers of different diameters is shown in figure 3.2a-3.2c. The figures were obtained by superimposing the image of the droplet taken after four hours of incubation on top of the image obtained after incubation for 24 hours. The edges of the droplet at the two time points are delineated by the solid lines. From the figure one can see that as the fiber diameter increases from 1, 4 to 8 microns the aspect ratio of the migration front increases. Closer examination of the area along the shorter axis shows that most of the cells comprising the front are migrating along the direction of the fiber orientation, hence the non-spherical distribution. As the fiber diameter increases one can see that the amount of cells migrating in a direction perpendicular to the fiber orientation decreases (inserts to figure 3.2a-3.2c), indicating that cell alignment along the fiber direction becomes easier as the fiber diameter increases.

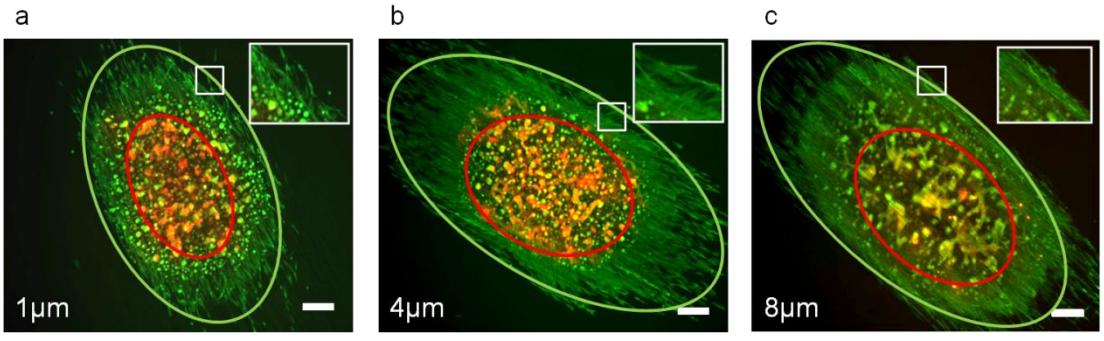

Figure 3.2 Fluorescent microscope overlap images of cells on different diameters of fibers. (Scale bar=400 μm)

In figure 3.3a-3.3c I show confocal microscopy of the cells migrating on fibers of different diameters where the focal adhesion points are imaged after complexing to an immunoflorescent stain for vinculin proteins. From the figure one can see that on the one micron fibers many cells are attached to more than one fiber. The focal adhesions seem to be distributed randomly on the cytoplasm, without regard to the underlying fibrillar structure. On the substrates with larger fiber diameters the cells are clearly oriented along the fiber direction, with nearly all the cells firmly attached to one fiber (figure 3.3d). A well-defined line of focal adhesion points is observed on most cells, which follows the contour of the fiber to which the cells are attached. The degree of orientation of the cells and the number of aligned focal adhesions increases with increasing fiber diameter.

In figure 3.3e I plot the migration velocity after 24 hours of incubation on fibers of different diameters. From the figure one can see that despite the lower number of focal adhesion points on the larger fibers, the migration speed decreases with increasing alignment along the fibers. Hence increased orientation also hinders the initial speed with which the cells emerge en mass from the droplet. This is consistent with the previous observation [11] where they reported that cells emerged en mass on oriented fibers at a lower speed than those on flat substrates as the cells waited in an orderly manner to find a place on the fiber.

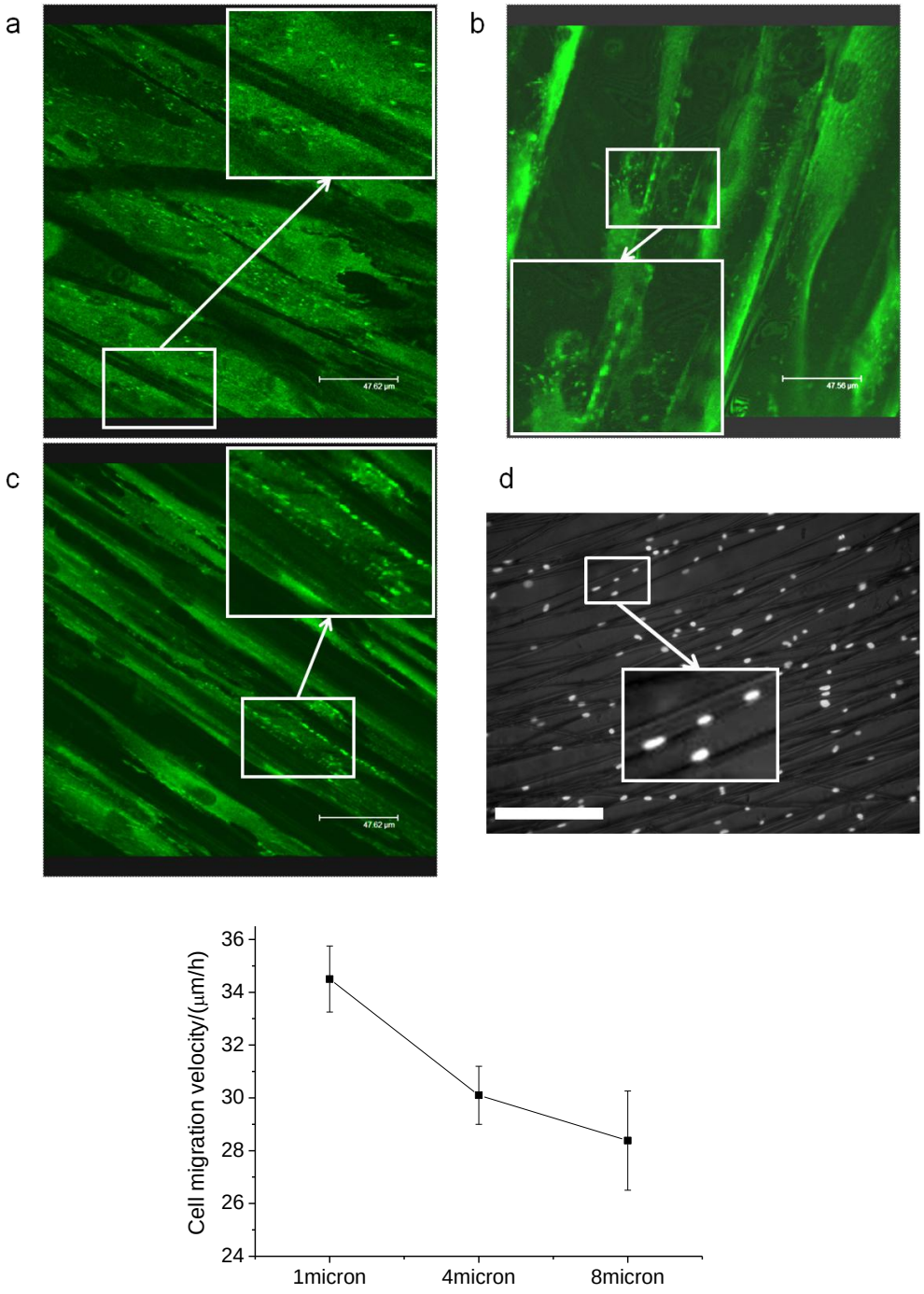

Figure 3.3 Cell migration on different diameter fibers. Confocal images of vinclulin on (a) 1µm, (b) 4µm, and (c) 8µm fibers. (d) Nuclei location on 8µm fibers (Scale bar=100 µm). (e) Cell migration velocity of on different diameter fibers.

3.3.2 Distance between fibers

The ability of all cells to find a position on a fiber when they emerge from the droplet can be thwarted if the distance between fibers is increased. In this case the pressure from other cells forces them out of the droplet in the space between fibers. In figure 3.4a I show a typical image of cells emerging on 8 micron fibers, approximately 100μm apart. From the figure one can see that a large number of cells are now in between fibers. In figure 3.4b I plot the number of cells between fibers at a fixed distance of 500-900μm from the droplet, as a function of the mean distance between fibers. From the figure one see that this number decreases with decreasing spacing and increasing distance from the edge of the droplet. In figure 3.4b I plot the migration speed of cells in the flat areas between fibers, as a function of inter fiber distance. From the figure I find that as the number of cells increases the migration speed decreases. This is in complete contrast with the behavior reported for en-mass migration of fibroblasts from a droplet, where the chosen trajectory is such as to maximize the distance between adjacent cells and to where the migration speed is highest at the largest cell densities. A closer observation of the cell migration dynamics in the space between fibers offers a possible explanation for this effect.

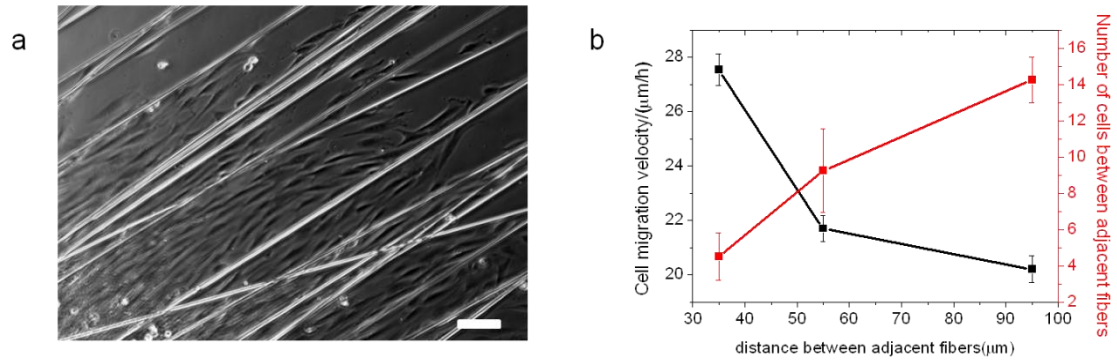

Figure 3.4 Cell migration on different spacing of fibers. (a) Phase contrast image of cells plated on 100 μm spacing fibers. (Scale bar=100 μm) (b) Cell migration velocity and number of cells as a function of spacing between fibers.

Fibroblasts extend long processes emanating from the cells on the fibers, where the process senses the local environment. As a result, cells on fibers will move in tandem, where table 3.2 lists the amount of neighboring cells whose motion may be correlated along one fiber or along adjacent fibers. Observation of the motion of the cells was shown in figure 3.5 and [supplementary material] that, in contrast to a flat open space where cells can move in random directions, the cells in the space between fibers also undergo correlated motion with a correlation number of approximately 3 cells. It is interesting to note that despite having emerged on the flat region of the sample, the cells somehow are aware of the presence of the fibers, and migrate towards the fibers. At that point, they slow down and wait for a space to present itself where they can attach to the fibers. As a result, the cell density on the flat areas decreases quickly with increasing incubation time and distance from the edge of the droplet.

	On the same fiber	On adjacent fibers
Spacing between fibers	Number of cells in correlation	Number of cells in correlation
~10μm	6.25±1.56	4.05±1.18
~30μm	4.05±0.93	2.93±1.53
~50μm	4.20±1.61	2.47±0.72

Table 3.2 Correlation distance of cells migrating on the same fiber and adjacent fibers.

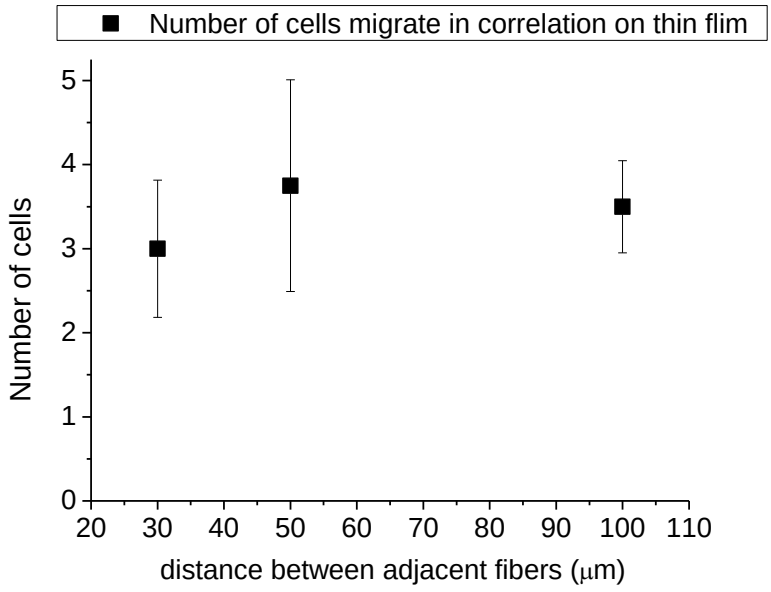

Figure 3.5 Number of cells migrate in correlation on the flat film between adjacent fibers.

3.3.3 Pattern formation

In order to migrate in three dimensions, cells must also be able to change course from fiber to fiber. I therefore also placed the agarose droplet on scaffolds where the fiber layers were arranged at a fixed angle relative to each other and observed the fraction of cells moving along the initial fiber direction relative to those which switched fibers and moved into another layer after 24 hours incubation (figure 3.6a). The geometry of the scaffolds was shown in figure 3.6b, where the distance between the aligned fibers was chosen to be approximately 30 microns.

From the figure one can see that the majority of the cells preferred continuing straight on the oriented fibers. Approximately 30% switched layers, when the scaffold angles were 30 and 45 degrees and slightly more, 35%, switched on scaffolds with a 90 degree angle. This can be seen even more clearly in figure 3.7 where I superimpose the initial droplet over the migration pattern that evolved after 24 hours. From the figure one can see that the patterns traced out reflect the ratio of cells emerging on layers placed at different angles. Clearly the cells chose to follow the fibers and move between layers only at junction points on the fibers, rather than coming off one fiber and moving onto the next in between junctions by extending on two fibers or via the flat spaces between fibers.

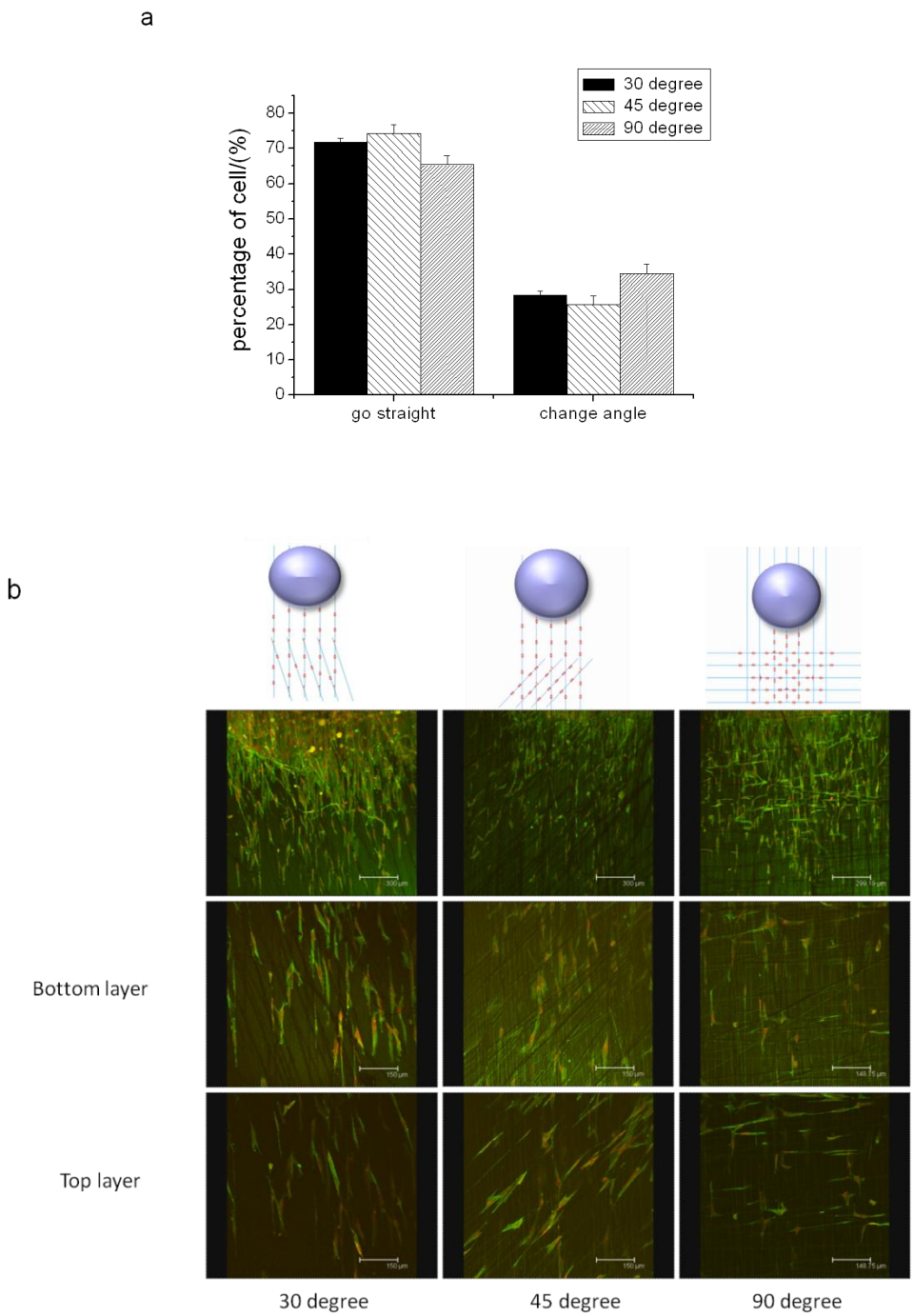

Figure 3.6 Cell migration on two layers of fibers. (a) Residence of cells on 30 ˚, 45˚, and 90 ˚ scaffolds. (b) Illustration and confocal images of cell migrating on 30 ˚, 45 ˚, and 90 ˚ scaffolds. (Green: F-actin, and red: nuclei).

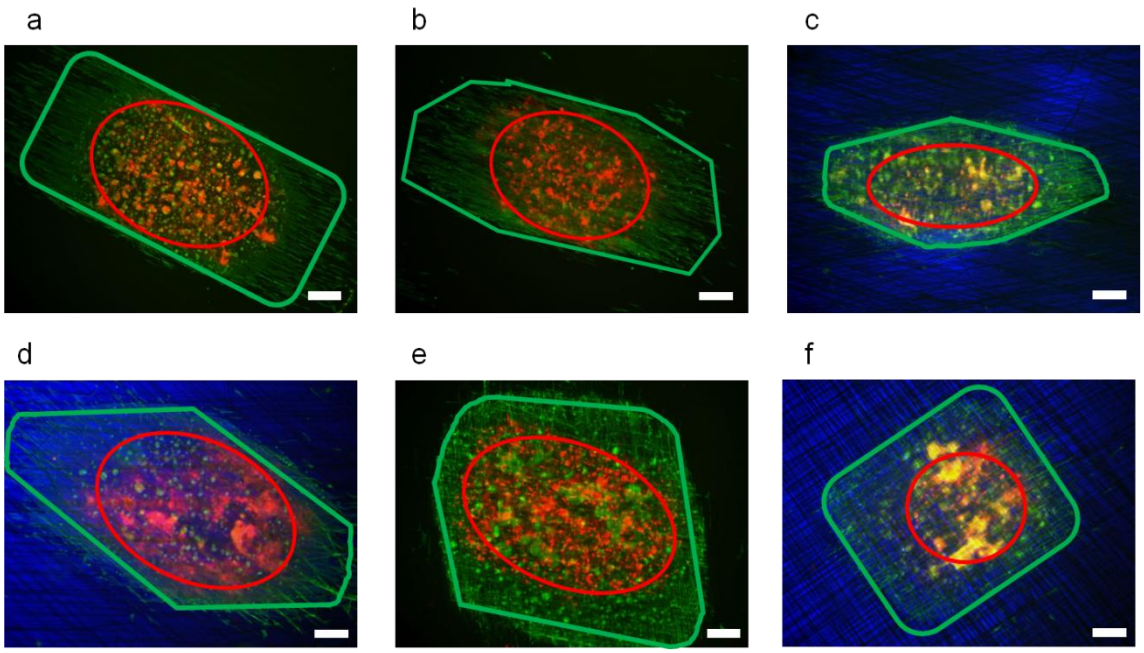

Figure 3.7 The overlapped image of en-mass cell migration of live cells stained with DiD (red), and incubated for four hours, onto the image of cells incubated for 24h, fixed and stained for F-actin with Alexa Fluor (green) on (a) 0˚, (b) 15˚, (c) 30˚, (d) 45˚, (e) 75˚ and (f) 90˚ scaffolds. (Scale bar: 400 μm)

3.3.4 Migration velocity

In figure 3.8a I plot the en-mass migration speed as a function of the angle between fibers in adjacent layers in the different scaffolds. From the figure I see that the migration speed has a parabolic form with respect to angle, with the maximum reduction in speed occurring at 30 degrees. This result was quite unexpected since one would predict that the degree with which the cells would slow down should scale with the deformation they would encounter in switching between fibers at the junction points. I therefore explored this phenomenon in more detail by observing the migration speed of individual cells as they approached a fiber/fiber junction and switched fibers, for the 30

and 90 degree scaffolds. From figure 3.8b one can see that on the 30 degree scaffold when the cells come within approximately 40 microns, they begin to slow down till they reach a value nearly half of their original speed at the junction itself. In contrast the cells on the 90 degree scaffolds migrate from one fiber to the next, undisturbed, at the same speed.

In figure 3.8c-3.8h I show confocal images of the cells 24 hours after emerging from an agarose droplet onto scaffolds with fibers oriented at 30, 45 and 90 degrees. In the inset I also plot SEM images of cells at the 30 and 90 degree junction points which show that they are well extended along the two fibers forming the junction with long processes extended along the fibers. Comparing these images with those shown above in figure 3.3c of the cells incubated for 24 hours on the oriented single layer substrate one can immediately see that the cells on the single layer substrate have more focal adhesion sites per cell. In the case of the cells migrating on the multi-layers substrates there are far fewer focal adhesions along the fiber perimeter and most seem localized along the junction region. This is consistent with the breaking of the focal adhesions on one fiber and reforming at the junction point in preparation of the cells changing direction. The spacing of junction points, approximately 40 microns, is roughly the same as the length of the cells, and hence the cells are constantly choosing their orientation direction, which may prevent the formation of the focal adhesion sites along the fiber perimeter and concentrating them at the junction. The number of focal adhesion sites per cell was plotted in figure 3.9a for 0, 30, and 90 degree scaffolds. From the figure one can also see that the number of focal adhesions is about 25% larger on the 30 degree scaffold than on the 90 degree scaffold ($p<0.01$) which is consistent with the

cells moving faster at the 90 degree junctions, having fewer focal adhesion complex to break as they change direction.

Nuclear deformation has also been reported as a driver for cell migration [26-29]. On flat surfaces migration was shown to occur as a consequence of redistribution of the traction forces as the cells attempted to reduce nuclear deformation. On fibers a permanent deformation is imposed via the orientation of the cells along the fiber axis. This is shown in figure 3.9b where the nuclei of the cells on the single layer substrate have an aspect ratio of 2.0. Measurement of the nuclear deformation of the cells at the junction points on the multilayer substrates shows that the nuclear deformation is maintained on the 90 degree scaffold, as the cells are changing direction, while it is reduced by 25% on the 30 degree scaffold while the cells are resident on the junction point indicating that the distribution of traction forces exerted by cells to change direction may also be a function of angle.

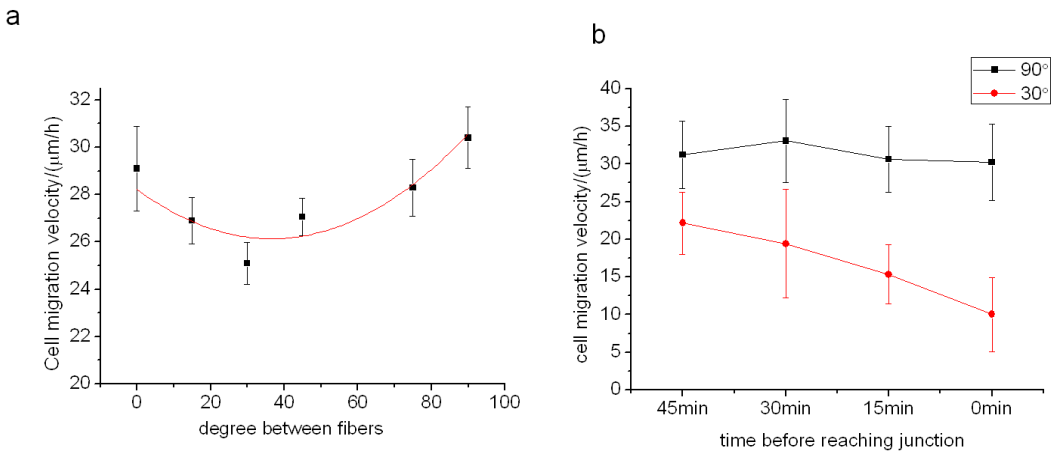

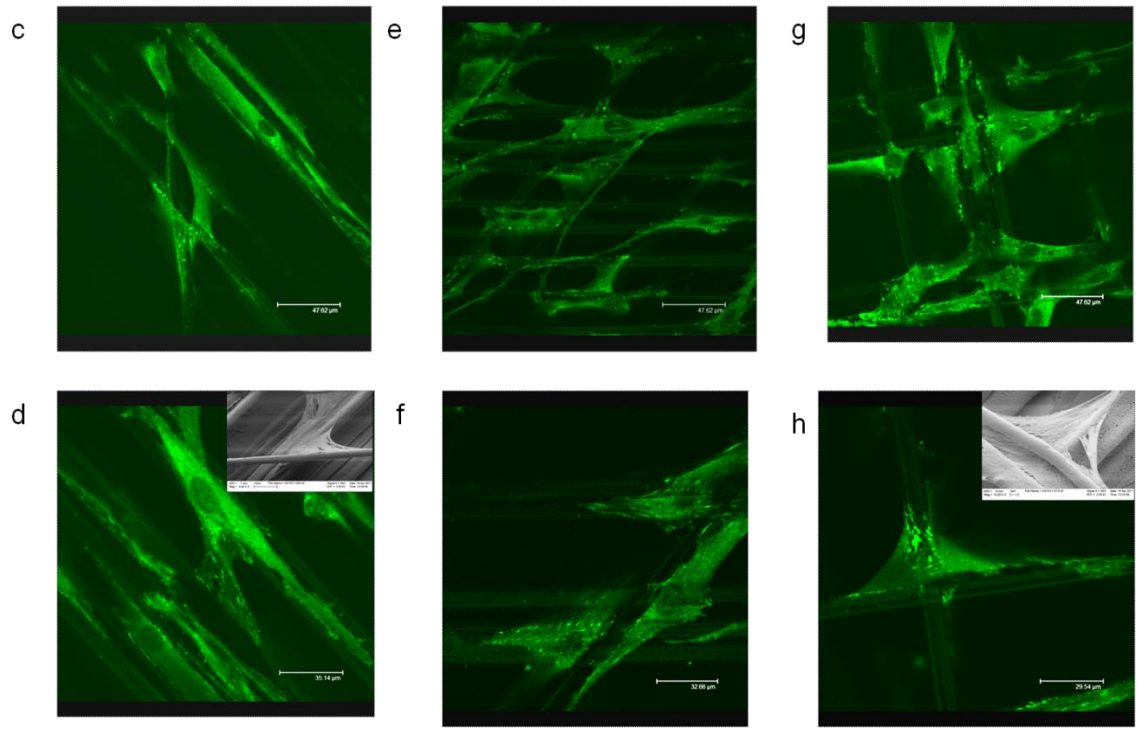

Figure 3.8 Cell migration on different angle scaffolds. (a) Cell migration velocity on electrospun fibers with different angles. (b) Migration velocity of cells approaching the junction on 30˚ and 90˚ surfaces. (c, d) Confocal images of vinculin on 30˚, (e, f) on 45˚ surfaces, (g, h) 90 ˚ surfaces (Inserts: SEM images of cells at fiber junction).

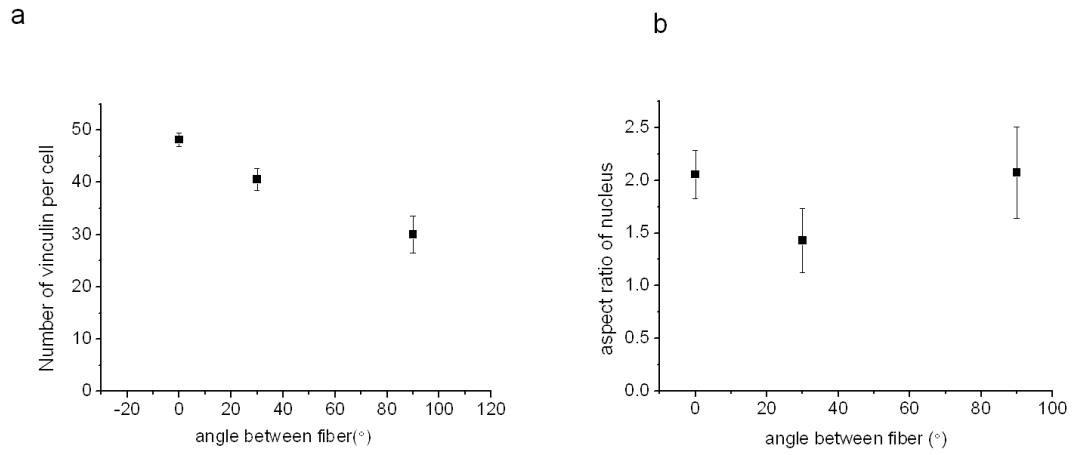

Figure 3.9 (a) Number of vinculin per cell on 30˚ and 90˚ surfaces. (b) Aspect ratio of nucleus on the surfaces.

3.4 Discussion

I have shown that dermal fibroblast cells strongly prefer migrating along fibers even when executing en-mass migration from an agarose droplet. This preference is established as soon as the cells emerged onto the fibers. Observation of the cells after 24 hours shows that the cells formed strong focal adhesion sites and are oriented along the fibers. The most pronounced degree of orientation occurred on fibers of diameter greater than 1 micron. Even though some degree of orientation was also observed on fibers one micron in diameter, rather than forming along the fiber, focal adhesions were observed throughout the cytoplasm and the degree of orientation was lower than on the larger diameter fibers. Measurements of the migration speed indicated that the cells migrated slower as the degree of orientation along the fiber increased. SEM images of the cells on the fibers showed large process also formed which extended large distances from the cytoplasm. These processes were very thin and were difficult to image using florescent stains. Nevertheless, these processes allowed the cells to sense the presence of other cells and resulted in highly correlated en-mass motion pattern. For cells emerging on flat films even though I observed en mass migration, no correlations were observed between individual cells, which migrated independently of each other. For cells migrating on the fibrillar surfaces a correlation length extending over approximately 4-6 cells along the fiber and approximately 2-4 cells in adjacent fibers was observed where the cells moved in a lock-step fashion. These multiple correlations were also thought to be responsible for the initial lower migration speed of the cells on the fibers relative to those on the flat films.

As the spacing between adjacent fibers increased, cells were forced to emerge from the droplet onto the flat films, in the space between the fibers. The number of cells in this region increased as the spacing between fibers increased but their migration speed decreased. This was in sharp contrast with the en-mass migration of cells on flat surfaces, without fibers, where the migration speed increased as the cell density increased. Closer observation of the migration pattern revealed that when fibers were present, even at a large distance, the cells in the flat regions migrated along a trajectory which eventually ended onto attachment to a fiber. In contrast to those cells migrating on the completely flat surfaces, the motion of these cells was highly correlated as well, with a correlation of approximately three cells. Hence in this case the long processes enabled the cells to sense the location of the fiber and coordinate the motion of nearby cells such that an orderly procession took place, where most of the cells in the flat space eventually attached to the fiber.

In order to observe three dimensional diffusion scaffolds with well defined angles between the fibers were formed and the en-mass migration out of the droplet was measured as a function of fiber angle. For fiber spacing less than 50 microns, nearly all the cells emerged on the fibers, regardless of direction, and moved vertically within the scaffolds by changing from one layer to the next only along the fiber junction points. Motion in three dimensions gave rise to distinct differences in the cell behavior. The frequent presence of the fiber junctions forced the cells along multiple migration trajectories, which interfered with the correlated behavior observed on the single layer scaffold. Furthermore, the frequent changes in orientation imposed at the junction points, also interfered with the formation of the long lines of focal adhesions which

formed along the oriented fibers. Instead, the focal adhesions were now concentrated along the junction points and long processes were observed to attach to the junctions allowing the cells to alter their migration speed or orientation in preparation of the approach. .

A very surprising detail was the observation that the migration speed on the multi-layer scaffold was a parabolic function of the angle between fibers in adjacent layers, with a distinct minimum in speed observed at an angle of 30 degrees. This minimum was consistent with the measurement with a 25 % increase in both numbers of focal adhesion points as well as a 25 % decrease in nuclear aspect ratio for cells migrating on the 30 degree scaffolds relative to those migrating on the 90 degree scaffolds. Cell migration has been shown to proceed via polymerization and de-polymerization of filaments followed by placement of focal adhesions [38-44]. Preferential angles involved in actin filament orientation have been reported by several groups where it has been shown that dendrites polymerizing on actin filaments form at a distinct angle of 70 degrees from the main filament backbone [45]. Recently it was also shown that cells subjected to cyclic stress deformation react by forming actin stress fibers oriented at 60 degrees to the stress direction [46, 47]. Hence, even though I do not have a model as yet, it is not surprising to find that cell re-orientation during migration should also have a pronounced angular dependence since it too is a process which also involves directional actin polymerization.

3.5 Conclusion

En-mass migration on fibrillar surfaces is an essential component of the wound healing process. I have therefore concentrated on studying the en-mass behavior of cells emerging from an agarose droplet onto single and multi- layered scaffolds of oriented fibers. On the single layered substrates I found that, for fibers with diameters greater than one micron, the cells formed focal adhesions oriented on the fiber axis and migrated along the fibers in a highly correlated manner. On the multi-layered scaffolds the en-mass migration speed was found to be a parabolic function of the angle between adjacent layers, with a well-defined minimum occurring at an angle of 30 degrees between adjacent layers. In this case the focal adhesions were concentrated at the fiber/fiber junctions with the number of adhesions being larger and the nuclear deformation being smaller than the corresponding values for those migrating on the 30 degree scaffolds relative those migrating on the 90 degree scaffolds, underscoring the role of fibrillar substrate alignment in orienting the collective migration of cells in three dimensions.

3.6 References

[1] Cheng Q, Lee BLP, Komvopoulos K, Li S, Engineering the Microstructure of Electrospun Fibrous Scaffolds by Microtopography, Biomacromolecules, 2013, 14: 1349–1360.

[2] Chen SH, Chang Y, Lee KR, Lai YJ, A three-dimensional dual-layer nano/microfibrous structure of electrospun chitosan/poly(d,l-lactide) membrane for the improvement of cytocompatibility, J. Membr. Sci, 2014, 450:224-234.

[3] Heydarkhan-Hagvall S, Schenke-Layland K, Dhanasopon AP, Rofail F, Smith H, Wu BM, Shemin R, Beygui RE, MacLellan WR, Three-dimensional electrospun ECM-based hybrid scaffolds for cardiovascular tissue engineering, Biomaterials, 2008, 29:2907-2914.

[4] Kim HN, Hong Y, Kim MS, Kim SM, Suh KY, Effect of orientation and density of nanotopography in dermal wound healing, Biomaterials, 2012, 33:8782-8792.

[5] McDougall S, Dallon J, Sherratt J, Maini P, Fibroblast migration and collagen deposition during dermal wound healing: mathematical modelling and clinical implications, Philos Trans A Math Phys Eng Sci, 2006, 364:1385-1405.

[6] Gupta T, Giangrande A, Collective cell migration: "all for one and one for all", J Neurogenet, 2014, 28:190-198.

[7] Woods ML, Carmona-Fontaine C, Barnes CP, Couzin ID, Mayor R, Page KM, Directional collective cell migration emerges as a property of cell interactions, Plos One, 2014: 0104969.

[8] Weijer CJ, Collective cell migration in development, J. Cell Sci, 2007, 122, 3215-3223.

[9] Olga Ilina, Peter Friedl, Mechanisms of collective cell migration at a glance, J. Cell Sci, 2009, 122, 3203-3208.

[10] Friedl P, Gilmour D, Collective cell migration in morphogenesis, regeneration and cancer, Nat. Rev. Mol. Cell Biol, 2009, 10, 445-457.

[11] Liu Y, Franco A , Huang L, Gersappe D, Clark RAF, Rafailovich MH, Control of cell migration in two and three dimensions using substrate morphology, Exp Cell Res, 2009, 315:2544-2557.

[12] Pan Z, Ghosh K, Hung V, Macri LK, Einhorn J, Bhatnagar D, Simon M, Clark RA, Rafailovich MH, Deformation gradients imprint the direction and speed of en masse fibroblast migration for fast healing, J Invest Dermatol, 2013, 133:2471-2479.

[13] Liu Y, Ji Y, Ghosh K, Clark RAF, Huang L, Rafailovich MH, Effects of fiber orientation and diameter on the behavior of human dermal fibroblasts on electrospun PMMA scaffolds, J Biomed Mater Res, 2009, 90A:1092–1106.

[14] Nikkhah M, Edalat F, Manoucheri S, Khademhosseini A, Engineering microscale topographies to control the cell-substrate interface, Biomaterials, 2012, 33:5230-5246.

[15] Brunette DM, Chehroudi B, The effects of the surface topography of micromachined titanium substrata on cell behavior in vitro and in vivo, J Biomech Eng, 1999, 121:49-57.

[16] Oakley C, Jaeger NA, Brunette DM, Sensitivity of fibroblasts and their cytoskeletons to substratum topographies: topographic guidance and topographic compensation by micromachined grooves of different dimensions, Exp Cell Res, 1997, 234:413-424.

[17] Kolind K, Dolatshahi-Pirouz A, Lovmand J, Pedersen FS, Foss M, Besenbacher F, A combinatorial screening of human fibroblast responses on micro-structured surfaces, Biomaterials, 2010, 31:9182-9191.

[18] Jeon H, Hidai H, Hwang DJ, Healy KE, Grigoropoulos CP, The effect of micronscale anisotropic cross patterns on fibroblast migration, Biomaterials, 2010, 31:4286-4295.

[19] Kaiser JP, Reinmann A, Bruinink A, The effect of topographic characteristics on cell migration velocity, Biomaterials, 2006, 27:5230-5241.

[20] Kim DH, Han K, Gupta K, Kwon KW, Suh KY, Levchenko A, Mechanosensitivity of fibroblast cell shape and movement to anisotropic substratum topography gradients, Biomaterials, 2009, 30:5433-5444.

[21] Diener A, Nebe B, Lüthen F, Becker P, Beck U, Neumann HG, Rychly J, Control of focal adhesion dynamics by material surface characteristics, Biomaterials, 2005, 26:383-392.

[22] Kim DH, Wirtz D, Focal adhesion size uniquely predicts cell migration, FASEB J, 2013, 27:1351-1361.

[23] Saunders RM, Holt MR, Jennings L, Sutton DH, Barsukov IL, Bobkov A, Liddington RC, Adamson EA, Dunn GA, Critchley DR, Role of vinculin in regulating focal adhesion turnover, Eur J Cell Biol, 2006, 85:487-500.

[24] Dumbauld DW, Shin H, Gallant ND, Michael KE, Radhakrishna H, García AJ, Contractility modulates cell adhesion strengthening through focal adhesion kinase and assembly of vinculin-containing focal adhesions, J Cell Physiol, 2010, 223:746-756.

[25] Dumbauld DW, Michael KE, Hanks SK, García AJ, Focal adhesion kinase-dependent regulation of adhesive forces involves vinculin recruitment to focal adhesions, Biol Cell, 2010, 102:203-23.

[26] Wang N, Tytell JD, Ingber DE, Mechanotransduction at a distance: mechanically coupling the extracellular matrix with the nucleus, Nat Rev Mol Cell Biol, 2009, 10:75-82.

[27] Friedl P, Wolf K, Lammerding J, Nuclear mechanics during cell migration, Curr Opin Cell Biol, 2011, 23:55-64.

[28] Wolf K, Te Lindert M, Krause M, Alexander S, Te Riet J, Willis AL, Hoffman RM, Figdor CG, Weiss SJ, Friedl P, Physical limits of cell migration: control by ECM space and nuclear deformation and tuning by proteolysis and traction force, J Cell Biol, 2013, 201:1069-1084.

[29] Pan Z, Ghosh K, Liu Y, Clark RA, Rafailovich MH, Traction stresses and translational distortion of the nucleus during fibroblast migration on a physiologically relevant ECM mimic, Biophys J, 2009, 96:4286-4298.

[30] Sorensent T B, Kjaer M, Agarose microdroplet leucocyte migration technique for detection of cell-mediated hypersensitivity to PPD and renal carcinoma antigen, Clin. Exp. Immunol, 1977, 30: 168-172.

[31] Morita C, Okada T, Izawa H, Soekawa M, Agarose Droplet Method of Macrophage Migration-Inhibition Test for Newcastle Disease Virus in Chickens, Avian Diseases, 1975, 20:230-235.

[32] Wiggins HL, Rappoport JZ, An agarose spot assay for chemotactic invasion, 2010, 48: 121-124.

[33] Liang CC, Park AY, Guan JL, In vitro scratch assay: a convenient and inexpensive method for analysis of cell migration in vitro, Nat Protoc. 2007;2: 329-333.

[34] Ashbya WJ, Zijlstra A, Established and novel methods of interrogating two-dimensional cell migration, Integr. Biol., 2012, 4, 1338–1350.

[35] Hulkower KI, Herber RL, Cell Migration and Invasion Assays as Tools for Drug Discovery, Pharmaceutics, 2011, 3, 107-124.

[36] Nain AS, Sitti M, Jacobson A, Kowalewski T, Amon C, Dry spinning based spinneret based tunable engineered parameters (step) technique for controlled and aligned deposition of polymeric nanofibers, Macromol Rapid Commun, 2009, 30:1406–1412.

[37] Nain AS, Phillippi JA, Sitti M, Mackrell J, Campbell PG, Amon C, Control of cell behavior by aligned micro/nanofibrous biomaterial scaffolds fabricated by spinneret-based tunable engineered parameters (STEP) technique, Small, 2008, 4:1153–1159.

[38] Kuo JC, Mechanotransduction at focal adhesions: integrating cytoskeletal mechanics in migrating cells, J. Cell. Mol. Med, 17, 2013 : 704-712.

[39] Hirata H, Tatsumi H, Sokabe M, Mechanical forces facilitate actin polymerization at focal adhesions in a zyxin-dependent manner, J Cell Sci, 2008, 121, 17:2795-2804.

[40] Ciobanasu C, Faivre B, Le Clainche C, Actin Dynamics Associated with Focal Adhesions, Int J Cell B, 2012, 2012: 941292.

[41] Schwarz US, Safran SA, Physics of adherent cells, Rev. Mod. Phys. 2013, 85: 1327.

[42] Puklin-Faucher E, Sheetz MP, The mechanical integrin cycle, J. Cell Sci, 2009, 122:179-186.

[43] Thievessen I, Thompson PM, Berlemont S, Plevock KM, Plotnikov SV, Zemljic-Harpf A, Ross RS, Davidson MW, Danuser G, Campbell SL, Waterman CM, Vinculin-actin interaction couples actin retrograde flow to focal adhesions, but is dispensable for focal adhesion growth, J Cell Biol, 2013, 202:163-177.

[44] Shemesh T, Geiger B, Bershadsky AD, Kozlov MM, Focal adhesions as mechanosensors: A physical mechanism, Proc Natl Acad Sci U S A, 2005, 102: 12383–12388.

[45] Mullins RD, Heuser JA, Pollard TD, The interaction of Arp2/3 complex with actin: nucleation, high affinity pointed end capping, and formation of branching networks of filaments, Proc Natl Acad Sci U S A, 1998, 95:6181-6186.

[46] Livne A, Bouchbinder E, Geiger B, Cell reorientation under cyclic stretching, Nat Commun. 2014, 5:3938.

[47] Qian J, Liu H, Lin Y, Chen W, Gao H, A Mechanochemical Model of Cell Reorientation on Substrates under Cyclic Stretch, Plos One, 2013, e 0065864.

Chapter 4 The role of oriented electrospun fibers in inducing continual cell deformation and the enhancement of cell migration velocity

4.1 Introduction

It has been nearly 20 years since Grinnell et al [1-4] first proposed that cell migration studies be performed in a 3-D collagen environment which mimics the human skin ECM. The ECM is a very complex system of fibers composed of a variety of different proteins such as collagen and fibronectin, whose sizes range from nanometer to micrometer. Cell migration, a critical process in wound healing, [5, 6] has been shown by numerous groups to be a function of substrate topography [7-12]. The micro-droplet technique is an accepted method for measuring cell migration, simulating wound healing, and allowing for the study of chemotaxis and haptotaxis. Yet, most studies, utilizing this method were performed on flat surfaces. In the case of fibroblasts, the sunburst patterns observed were shown to result from haptotaxis as the cells try to maximize the distance between adjacent cells. Liu et al [13] compared the migration of cells on flat surfaces to that on fibrous mats and found some fundamental differences. Measuring the migration velocity as a function of distance from the droplet, over a period of 24 hours, they found that on flat surfaces, the cells move fastest as they exit the droplet, but slow down as the distance between them increases, reaching a terminal velocity similar to the single cell value. When the droplets were placed on a mat of parallel fibers with diameters greater than 8 microns, the cells organized to form a ring around the perimeter of the droplet, and exited by moving only along the fibers. Therefore, for the first 24 hours, the distance between cells remained constant with time, being determined by the fiber pattern rather than the cell trajectory. The cell velocity also remained constant at the single cell value, which was much lower than the exit velocity on the flat film.

McClain et al studied the time scale for healing of punch wounds in a Yorkshire pig model and found a three day lag period before the onset of granulation tissue formation [14]. Since granulation tissue forms via en mass fibroblast cell migration, I wanted to investigate the nature of the cell velocity on different substrates after the first 24 hours. Even though the in-vivo process is more complex, being the result of multiple factors, here I focused on the influence of substrate morphology by measuring the migration for up to seven days and correlating the results with changes in cell and nuclear morphology, cell metabolism, and expression of vinculin and myosin IIA.

4.2 Materials and Methods

4.2.1 Hydrogel substrates preparation

Clean glass coverslips were coated with a thin film of PMMA (Mw=120,000 Da, Mw/Mn = 3; Sigma-Aldrich inc., St Louis, MO) which were spun cast from toluene solution ((Fisher Scientific, Pittsburgh, PA) at a concentration of 30mg/mL by at 2500PRM for 30 seconds. Samples were then annealed at 120°C in a vacuum of 10^{-7} Torr overnight to remove the remaining solvent, remove stress in the film, and sterilize the substrates. Fiber scaffolds were generated by electrospinning different PMMA solution and colleting by a rotating drum at 6750 r/min. Before seeding the cells, all samples had been sterilized under ultraviolet (UV) light for 20 min. Then, a solution of 30μg/ml intact human plasma fibronectin (Fn) (Millipore, Temecula, CA) solution in serum free Dulbecco's Modified Eagle medium (DMEM) was added at 37°C for 2 h.

4.2.2 Cell culture and cell migration assay

Adult Human Dermal Fibroblasts (CF29) were purchased from ATCC, and the experiment only used cell passages from ten to twelve. Cells had been routinely cultured in Dulbecco's Modified Eagle medium (DMEM), with 10% fetal bovine serum (Hyclone, Logan, UT) and antibiotic mix of penicillin, treptomycin, and L-glutamine (GIBCO BRL/Life Technologies, Grand Island, NY) in a humidified incubator at 37°C. The traditional agarose gel migration assessment was performed. The membranes of fibroblasts were stained with DiD dye, and then re-suspended in a volume of 0.2% (w/v) agarose solution to obtain the final cell density of 1.5×10^7 cells/ml. The agarose droplet was then introduced to the sterilized sample with micropipette, and each droplet was of 1.25μL. Samples with cells were then placed at 4 °C for 10 min to allow the agarose to solidify. After cooling, full- DMEM was added to each sample. Cells were then cultured in the 37°C incubator with 5% CO_2 for 4 days.

4.2.3 Measurement of cell migration speed

Time-lapse images of fibroblasts cell migration are recorded by MetaMorph®-operated CoolSNAP™HQ camera (Universal Imaging Corporation, Downingtown, PA) attached to a Nikon Diaphot-TMD inverted microscope fitted with a 37 °C incubator stage and a 10× objective lens. Images were automatically taken each 15 min and for total 60 min, so 5 pictures were taken every time. Migration velocity could be calculated by measuring the total migration distance divided by migration time. Single cells that were at the leading edge of migration were chosen because they there are no cell-cell

interference. Dividing cells and those that were out of focus plane are excluded. Final data was calculated after repeating the above experiment for at least 4 times and measuring at least 20 cells, with 3 replicates.

4.2.4 Immunofluoresent staining

Cells were rinsed with PBS, fixed with 3.7% formaldehyde for 20 min, then permeabilized with 0.4% Triton for 7 min, and blocked with 2% BSA in PBS for 30 min at room temperature. Focal adhesions were visualized by immunostaining for vinculin (Sigma, Saint Louis, MO), at a 1:600 dilution for 1 h then incubated with the Oregan Green 488 goat anti-mouse secondary antibody (Invitrogen, Carlsbad, CA) at a 1:600 dilution for 1 h at room temperature. Similar method was used for the myosin IIA (Cell Signaling Technology, Danvers, MA) staining. Nuclei were stained with 4',6-diamiadino-2-phenylindole (DAPI, Sigma-Aldrich, Inc., St. Louis, USA) for 10 min at room temperature. F-actin was stained with phalloidin (Invitrogen, Carlsbad, CA) for 20 min. Samples were then imaged by a Leica TCS SP2 laser scanning confocal microscope (Leica Microsystems, Bannockburn, IL) with water objective lens. The number of vinculin-positive focal adhesion sites, the aspect ratio of nuclear, and the intensity of mysion IIA staining were quantified by Image J.

4.2.5 XTT assay for cell metabolism

The standard XTT assay kit was purchased from Roche (Indianapolis, IN), and followed the company procedure. The initial cell density was 2500cells/well with 400 μL medium. After 4 days incubation, a mixture with 50:1 ratio of labeling reagent and electron-coupling reagent was added to the medium and detected by an Bio-RAD microplate reader (Hercules, CA) at 450 nm after 4 hrs in a humidified incubator.

4.3 Results and discussion

4.3.1 Migration Speed

In figure 4.1a, 4.1b I show fluorescent microscope images of the droplet and the cells emanating from the droplet onto spun cast flat PMMA film substrates and parallel electrospun PMMA fibers, both coated with fibronectin. The images are formed by a superposition of the image taken after four hours (red, DiD), onto the image of cells obtained after incubation for an additional 24 hours, after which the cells are fixed and stained for F-actin with Alexa Fluor (Green). From the figures one can see that immediately upon emergence, the pattern of the migration differs between the cells on the flat film and the cells placed on the fibers. Since the chemical composition of the two types of substrates is the same, the differences reflect primarily substrate topography and are a consequence of the confinement of the cells. The cells on the flat film form a sunburst pattern as they emanate from the droplet (figure 4.1a), where their trajectories reflect a tendency of fibroblasts to migrate away from each other. In contrast, those

coming out from the droplet placed on the fibers (Figure 4.1b), orient themselves along the fibers and migrate only in the fiber direction. The velocity, as measured from the distance traveled from the droplet edge to the perimeter of the migrating cells, is plotted as a function of time in figure 4.1c. From the figure I find that the cells emerge from the droplet with an initial velocity which is approximately 60% greater on the flat than on the fibrillar surface. With increasing time, the distance between cells increases and the migration velocity decreases, approaching the single cell value after 24 hours. In contrast, the cells placed on the fibrillar substrate emerge from the droplet with the single cell migration velocity, which remains constant for the first 24 hours. These results are consistent with those previously reported study [13] where they explained their results in terms of a haptotaxis like phenomenon due to cell crowding, as opposed to a chemotaxix effect where soluble factors were present. Fibroblasts put out cell processes which can sense adjacent cells. On the flat surface, the cells chose a trajectory which would continuously increase the distance between cells. The largest speed was observed at the smallest cell-cell distance. On micron sized fibers, once the cells emerged from the droplet, the cell-cell distance was determined by the fibers which on the oriented fiber surface remained constant with minimal cell-cell contact. Hence in the absence of a haptotaxic gradient, the cell migration speed remained constant at the value of the single isolated cell for the first 24 hours.

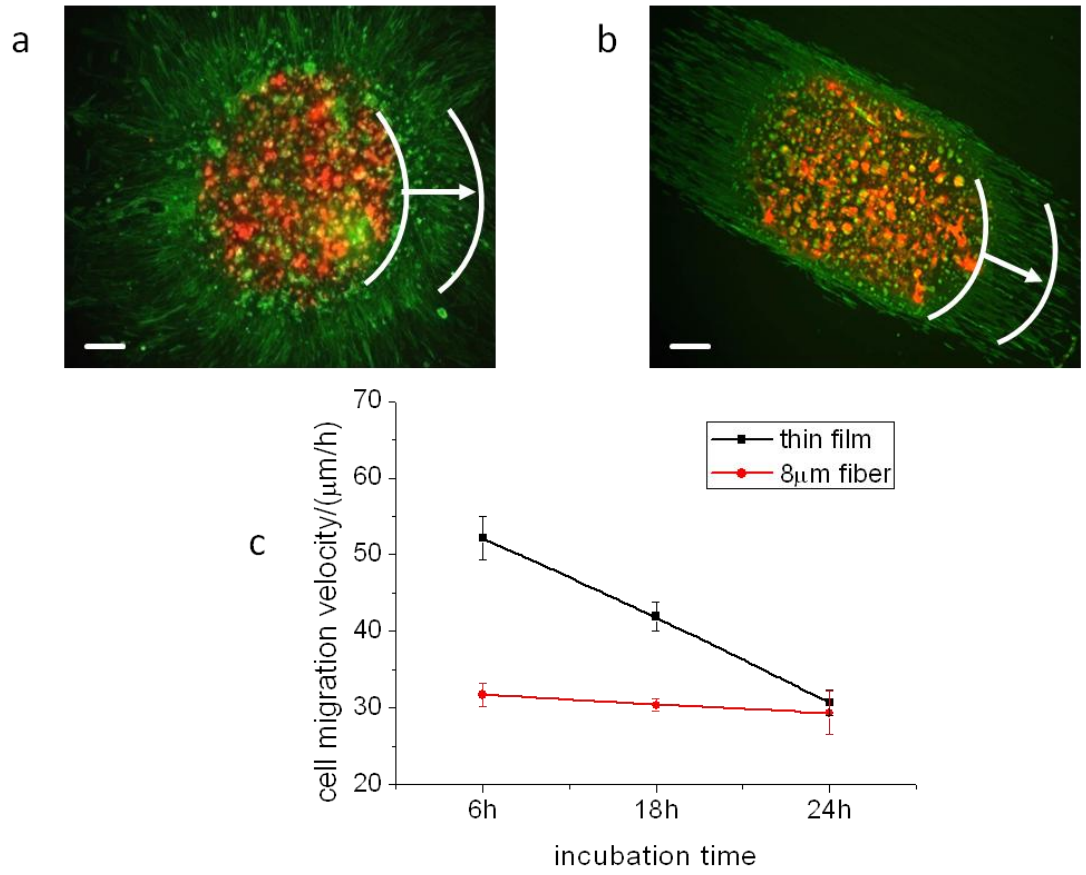

Figure 4.1 En-mass cell migration within 24 hours. The overlapped image of en-mass cell migration of live cells stained with DiD (red), and incubated for four hours, onto the image of cells incubated for 24h, fixed and stained for F-actin with Alexa Fluor (green) (a) On a spun cast, FN coated PMMA thin film and (b) On electrospun FN coated, PMMA microfibers. The lines are drawn to guide the eye towards the perimeter of the migration front at 4 and 24 hours, respectively. Error Bar= 250 μm. (c) The en-mass cell migration velocity, as measured from the motion of the front, on the thin film (black) and 8μm fibers (red) as a function of time.

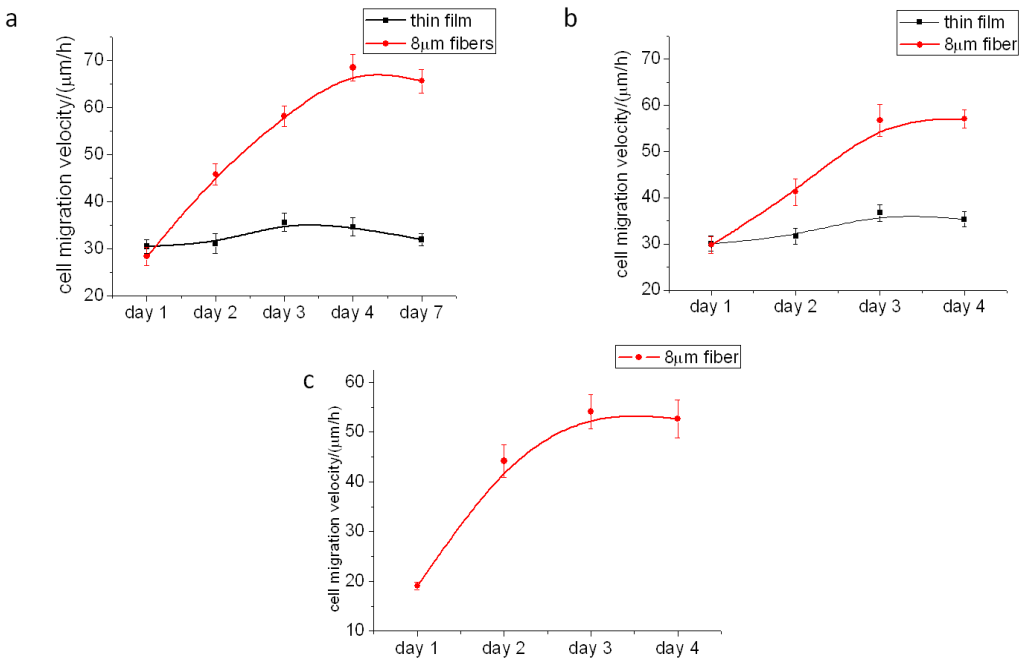

Figure 4.2 Cell migration velocity after 24 hours under different conditions. (a) En-mass cell migration velocity on FN coated thin film and 8μm fibers. (b) Single cell migration velocity on FN coated thin film and 8μm fibers for 4 days. (c) En-mass cell migration velocity on collagen coated thin film and 8μm fibers for 4 days.

In figure 4.2a I plot the migration speed, measured at 24 hour intervals, during the subsequent three days following the initial 24 hours. From the figure one see a dramatic reversal of the response. The cells migrating on the flat films are now moving at the constant single cell velocity, while those in the fibrillar surfaces are accelerating at a constant rate of $|a|=4.3\times10^{-5}$nm/sec^2, reaching, by the fourth day, a velocity nearly double the single cell value of v=68.5 μm/h, and exceeding the initial velocity of those on the flat surfaces. Further measurements from day 4 to day 7, show that no further change in the velocity on both flat and micron fiber substrates.

In order to rule out any chemotaxic or haptotaxic effects from the droplet, I also measured the single cell migration speed with incubation time, where cells were plated

directly on the substrate at an initial cell density of 2500cells/well without the agarose droplet. The results are shown in figure 4.2b, where I find that on the flat surfaces the magnitude of migration speed after 24 hours is the same as which achieved by the cells that had migrated out of the droplet, confirming that the cells migrating on the perimeter of the droplet had achieved single cell behavior. The response of the cells to increasing incubation time is also similar to that observed when the cells are initially plated within the droplet, namely the migration speed of the cells plated on the flat films remains constant for the four day observation period, while the speed of the cells plated on the fibrillar surface increases with the same constant rate of $|a|=4.5\times10^{-5}nm/sec^2$. The only difference between the cells plated directly on the substrate and those emanating from the droplet, is the magnitude of the plateau speed=59.1μm/h which is reached at day 3, rather than day 4, and is similar to the value 52.2μm/h of the cells existing the droplet on the flat surface. Hence the increase in migration speed appears to be caused by the fibrillar topography of the substrate rather than a consequence of the en-mass behavior of the migration imposed by the crowded condition in the droplet.

In order to rule out any effects specific to fibronectin, the fibers were also coated with collagen and the en mass velocity of the cells emanating from a droplet was measured as a function of time. From the results are plotted in figure 4.2c, where one can see that even though the initial velocity is somewhat lower, the functional behavior is similar to the single cell response shown in figure 4.2b. The migration velocity increases linearly, reaching a plateau at v=60.0μm/h on the third day, and hence the phenomenon is not related to activation via any functional domains specific to fibronectin.

4.3.2 Morphology and metabolic activity

Observation of the morphology of the cells plated on the flat and fiber surfaces shows that the cells on the flat surface have multiple orientations, which are continuously changing during the migration process, while those on the fibers remain orientated along the fiber direction. In figure 4.3a I plot the time averaged aspect ratio of the cells at day 4 on the flat and fibrillar surfaces, where I see that the value on the fibrillar surfaces is significantly larger, 7.1 vs 5.1 ($p<0.001$).

In order to determine whether placement of the cells on the fibers affects the rate of metabolism, an XTT assay, was performed on day 4, and as shown in figure 4.3b, no significant differences were observed between the cells plated either on the flat surfaces versus the electrospun fiber surfaces. Hence no additional mitochondrial activity occurs as a result of the cell continuously conforming to the three dimensional topography of the fibers.

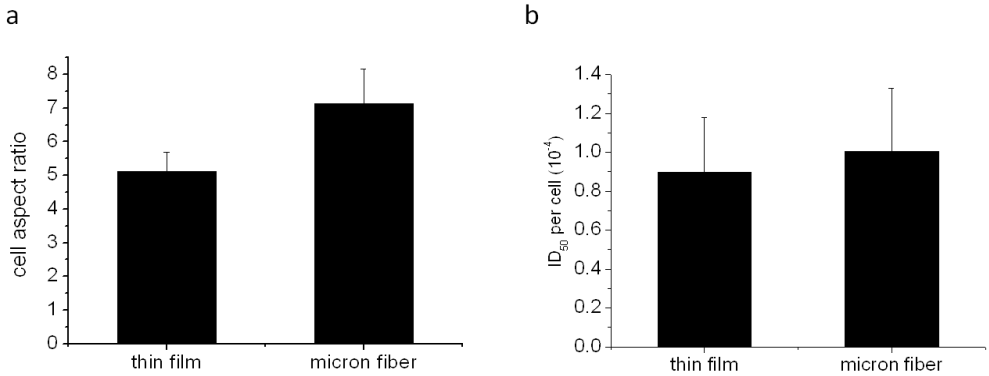

Figure 4.3 Cell aspect ratio and ID_{50} per cell reading on thin film and microfibers at day 4. (a) Cell aspect ratio was calculated as: the length of the cell/width of the cell plated

on thin film and micron fiber surfaces. (b) The XTT assay at day 4 was performed and followed with a DAPI nuclear staining. The reading of ID_{50} value reflects the metabolism level of all the cells at day 4. However, the cell proliferation varied on different surfaces. As a result, I divided the ID_{50} value by the actual nuclear number counted after DAPI staining, and evaluate the metabolism level per cell.

4.3.3 Localization of vinculin

The migration velocity is closely related to the number and size of focal adhesion sites for the cells on the substrate [11, 15, 16]. To achieve the maximum velocity, cells must be able to form optimal strength of focal adhesions. If the adhesion is too strong cells will migrate at a low speed, and if the adhesion is too weak, cells will not be able to exert adequate traction forces and will be unable to migrate. A recent study has shown that the size of the focal adhesions may be correlated to the cell migration [17]. I therefore, stained the cells with immunoflorescent antibodies against vinculin, obtained images with confocal microscopy, and the results are shown on figure 4.4a, and 4.4b. From the figures, one can immediately see that the pattern of focal adhesion contacts, as determined from the vinculin stain, varies drastically between the cells plated on the flat films and those plated on the 8μm fibers. On the flat films one can see focal adhesions distributed both at the periphery of the cells as well as on the interior, whereas on the 8μm fibers the focal adhesions were clustered only along the edges, following the contours of the fibers. The distribution of the focal adhesion points can be quantified by plotting the percentage of the focal adhesions present at different distances from the cell edge. The results are shown in figure 4.4c, where one can see that on the flat surface only approximately 20% are within 5μm of the cell edge, with the remainder distributed almost uniformly up to 35μm from the edge. On the fibers more

than 60% are within 5μm, with a sharp decrease to only a few percent at 10μm from the edge. The distribution of loci of the focal adhesions may reflect the mechanism of motion of the cells. On the flat surfaces the cells migrate either radially outward from the droplet or along random directions, following processes which may be extend in all directions. On the fibers though, motion occurs in only along the fiber, and the cell shape is defined by the edge of the fiber.

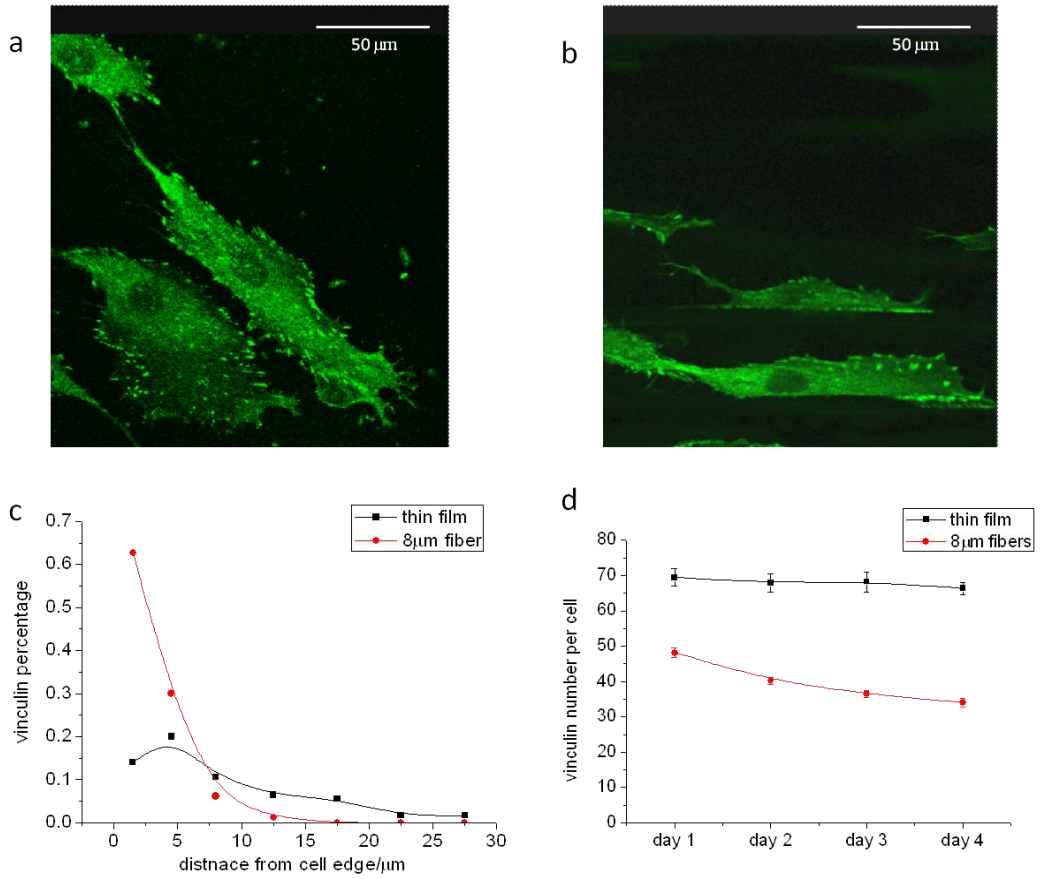

Figure 4.4 Vinculin distribution on flat film and 8μm fibers. (a) Confocal images of vinculin distribution on thin film at day 4 (b) Vinculin distribution on 8μm fibers at day 4. (c) The distribution of vinculin as a function of distance from cell boundary at day 4. The percentage of vinculin number was plotted as a function of the distance between vinculin locations to the edge of the cell. (d) The number of vinculin per cell on different surface for 4 days.

The number of focal adhesion points per cells was also counted and the results are plotted in figure 4.4d as function of incubation time. From the figure we see that the number of focal adhesion per cell on day one is 70 on the flat films vs. only 50 on the 8μm fibers, even though at this time the migration velocities on the two substrates are nearly the same. With increasing incubation time the number on the flat films remains constant while the number on the 8μm fibers decreases gradually to 35 by the fourth day. The decrease in focal adhesion number is consistent with the increase in migration speed during the same period of time on the 8μm fibers. The lack of change in number on the flat surface is consistent with the lack of change in the speed of migration on these substrates.

4.3.4 Aspect ratio of the nucleus

In the previous study, I have shown that on flat surfaces, migration was triggered by nuclear deformation [18], which initiated a cycle of traction force exertion to reduce deformation and ultimately resulted in center of mass translocation. Conversely, it was recently shown that inhibition of nuclear deformation via physical constraints led to complete cessation of cell migration [19]. I therefore investigated whether nuclear deformation may also be involved in triggering the enhanced migration on the fibrillar surfaces.

In order to observe the nuclear structure I stained the nucleus of cells cultured on the different substrates with DAPI, and their aspect ratio was measured (figure 4.5a-4.5d).

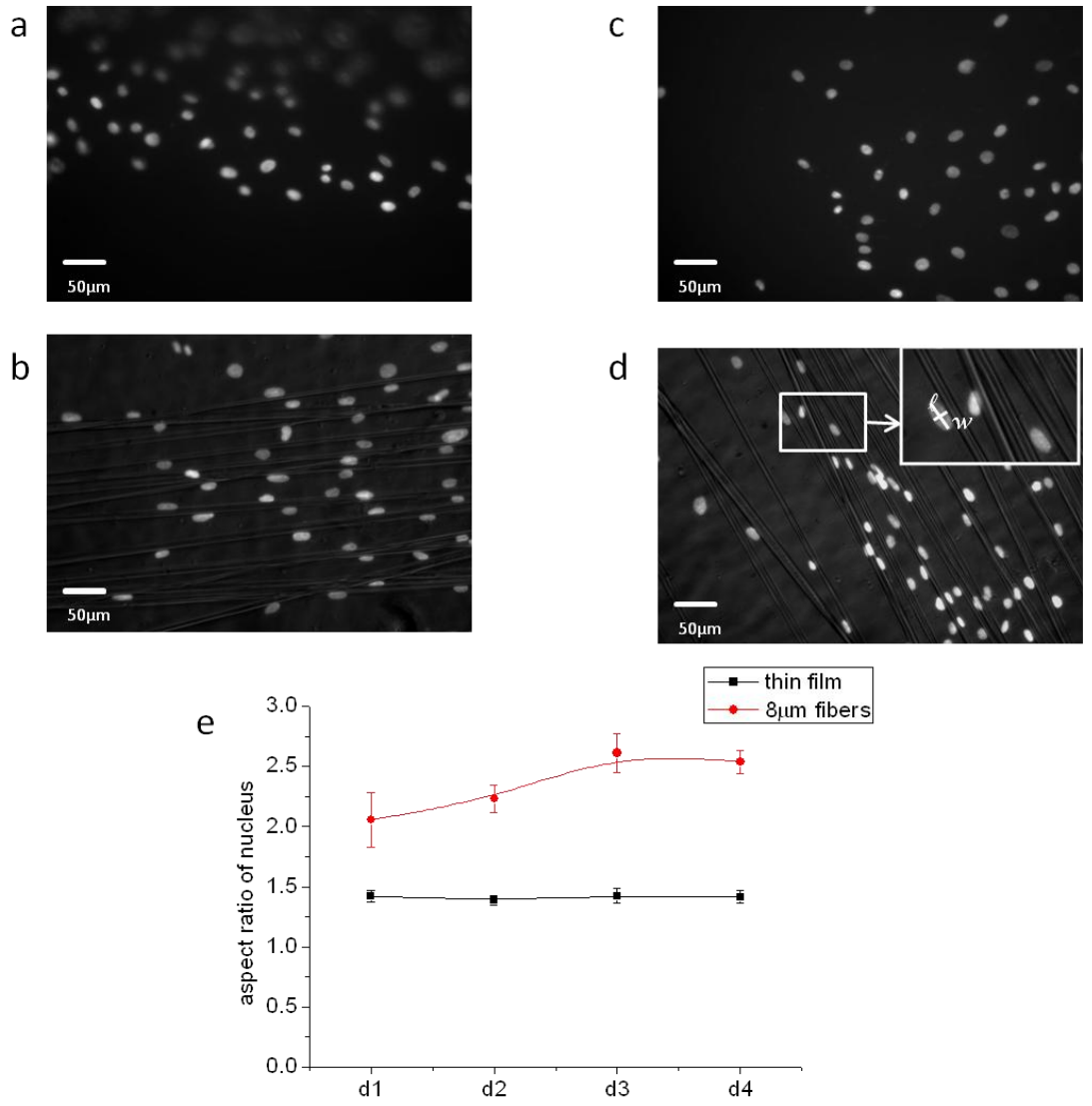

Figure 4.5 Nuclei morphology on different surfaces. The nuclei morphology at day 1 on (a) thin film (b) 8μm fibers, (c) Nuclei morphology at day 4 on thin film (d) 8μm fibers. (e) Measurement of cell aspect ratio on different surfaces for 4 days.

From figure 4.5e, I found that the nuclei of the cells on the flat films ranged from spherical to slightly (Rmax~2.1) elongated, with the mean elongation R~1.4 remaining constant over the four day observation period. The relatively large dispersion reflects

the fluctuation in nuclear aspect ratio previously reported by Pan et al to be associated with different stages of the migration process on flat surfaces. On the fibrillar surfaces the aspect ratio was larger immediately after the cells exited from the droplet, with an average value of R=2.0 after 24 hours. This value increased gradually reaching a plateau of R=2.5 on the third day. Since nuclear deformation is a vital part in cell migration, [20-22] it is tempting to postulate that it may be responsible for the acceleration of the cells on the fibers, where nuclear deformation is observed to increase during the same period as the cell migration velocity increases. In contrast, on the flat surfaces, both the mean velocity and the mean nuclear deformation remain constant over this period of time.

4.3.5 Intensity of myosin IIA and cell contraction

Myosin IIA is another important protein associated with cell migration since it plays a large role in transmitting the traction forces responsible for cell contraction as well as nuclear deformation [23, 24] during migration. Traction forces are transmitted via fiber bundles consisting of actin/myosin complexes where the actin fibers are contracted via connections to the myosin, hence transmitting forces due to focal adhesions with the surface [25-29]. In addition Myosin II also regulates vinculin recruitment and focal adhesions, which in turn determine migration velocity [30]. In order to observe Myosin fiber formation I stained the cells with immunofluorescent antibodies against Myosin IIA. I chose Myosin IIA over Myosin IIB since it is more prominent [31] in generating forces in nonmuscle cells. The results are shown in figure 4.6a for cells on the 8μm fibers and on flat substrates. In all images I found uniform myosin staining across the cell

cytoplasm, where the intensity does not vary significantly between cells plated on flat or fiber surfaces that incubated for one or four days. This finding is consistent with the RT-PCR data (figure 4.6b) where no significant differences were detected in the levels of Myosin IIA RNA.

Closer examination of the images (expanded segment of typical cells) show that on day one the myosin is organized into thin fibrils, approximately 0.7μm in diameter, which are extended across the long axis of the cell. These fibrils appear on all samples but are more pronounced on the flat surfaces. In figure 4.6a I show the corresponding images for the cells, which also stained for F-actin. Comparing the figures, one can see that the distribution of the thin myosin fibers parallels that of the actin fibers which is consistent with the formation of the actin/myosin complexes reviewed in the literature [24, 32].

The appearance of the cells on the flat substrates does not change much between days 1 and 4. On the other hand, on the fibrillar surfaces, much thicker fibers become visible which span the length of the cells, and are oriented parallel to the underlying direction of the 8μm fibers. Even though these fibers appear brighter, the intensity ratio of actin to myosin is not significantly different from the thinner fibers, indicating that they consist of similar actin/myosin complexes. The average diameters measured for the actin/myosin complies on the flat and fibrillar surfaces on days 1 and 4 are compared in figure 4.6c.

It has been demonstrated by numerous groups [32-34] that actin/myosin fibers are responsible for the exertion of traction forces which in turn mediate the process of

cell contraction and translocation of the cell center of mass. I therefore measured the average amount of cell contraction on day 1 associated with migration and the degree of contraction associated with the migration on day 4 (figure 4.7a). From the figure one can see that the degree of contraction on day 1 on the fibrillar surface resembles that on the flat surface, but by the fourth day the degree of contraction on the fibers had nearly doubled, while the one on the flat surfaces remains unchanged.

Examination of the moving images of the cells taken on days 1 and 4 (supplementary materials) shows that this difference in contraction is a result of a complex set of motions which the cells undergo and which ultimately result in nuclear translocation or cell migration. In figure 4.7c, I illustrate the processes that are observed in the supplementary videos of the migrating cells. The motion on the flat surface was observed a “fluttering” of the cytoplasm as the cell extends processes in multiple directions. Then as discussed in previous paper [18] I find that the nuclear shape changes abruptly, becoming more symmetric, which then causes retraction of the rear of the cell and nuclear translocation. Initially similar type of motion is observed on the fibrillar surface. On this surface one sees that most cells have one side attached to the sides of the fibers, while the other side is fluctuating freely. Initially, (first 24 hours) cell migration is similar on both types of surfaces but with increasing time the cells on the electrospun fibers appear to switch to a different mode. Instead of putting out processes in random directions, they are committed to following the direction of the fiber, and fluctuations of the periphery of the cytoplasm are no longer apparent. Hence the appearance of the large diameter of actin/myosin fibers also coincides with the increase in cell contraction and the rapid highly oriented motion.

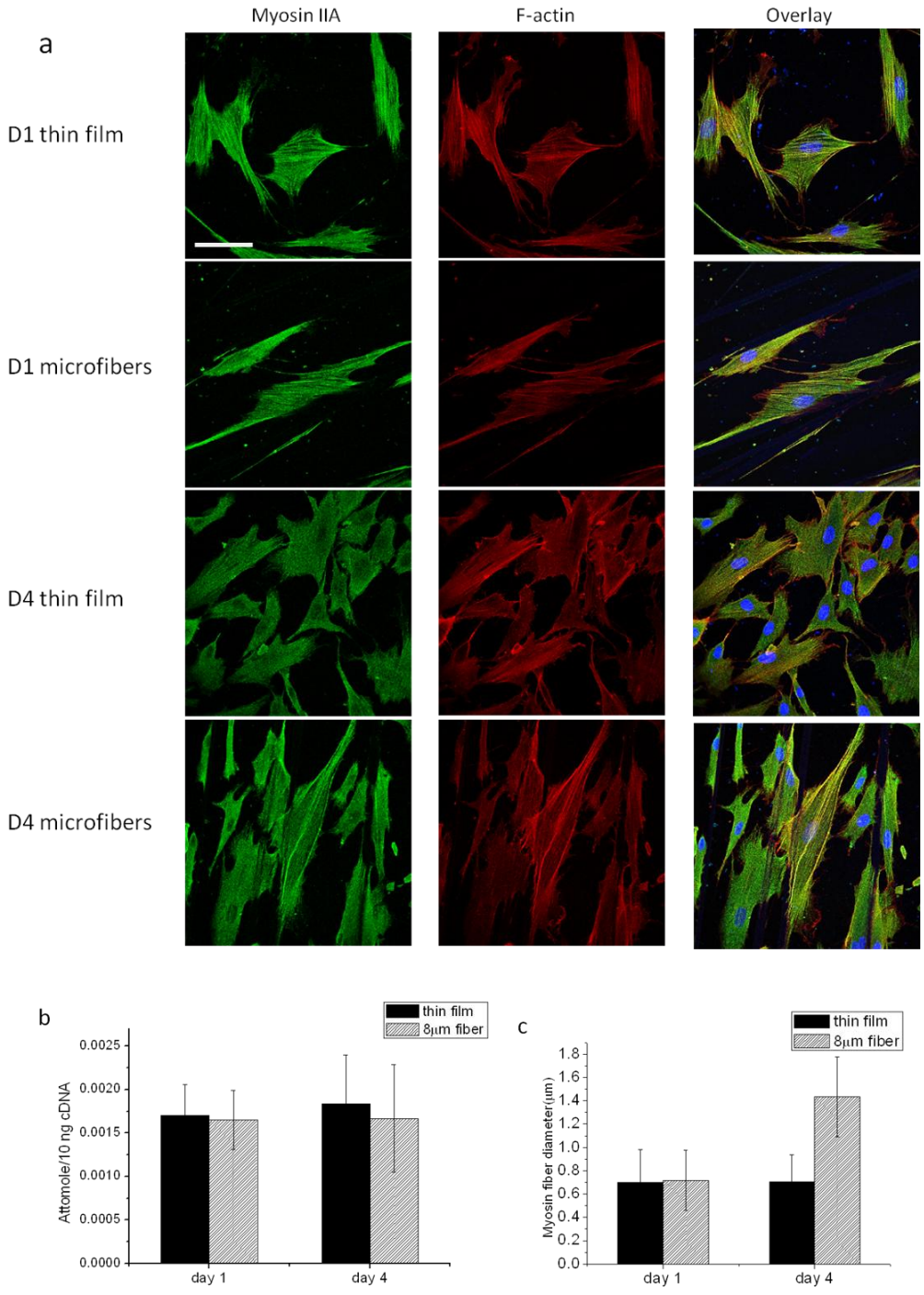

Figure 4.6 Immunofluorescent staining, RNA expression, and fiber diameter of Myosin IIA at day 1 and day 4. (a) Confocal images of cells stained with myosin IIA (green), F-actin (red), and the merged pictures on thin film and 8μm fibers. Error bar=75μm. (b)

RT-PCR result of MyosinIIA (2208F-2440R) expression on thin film and 8μm fibers. (c) Myosin fiber diameter on thin film and 8μm fibers.

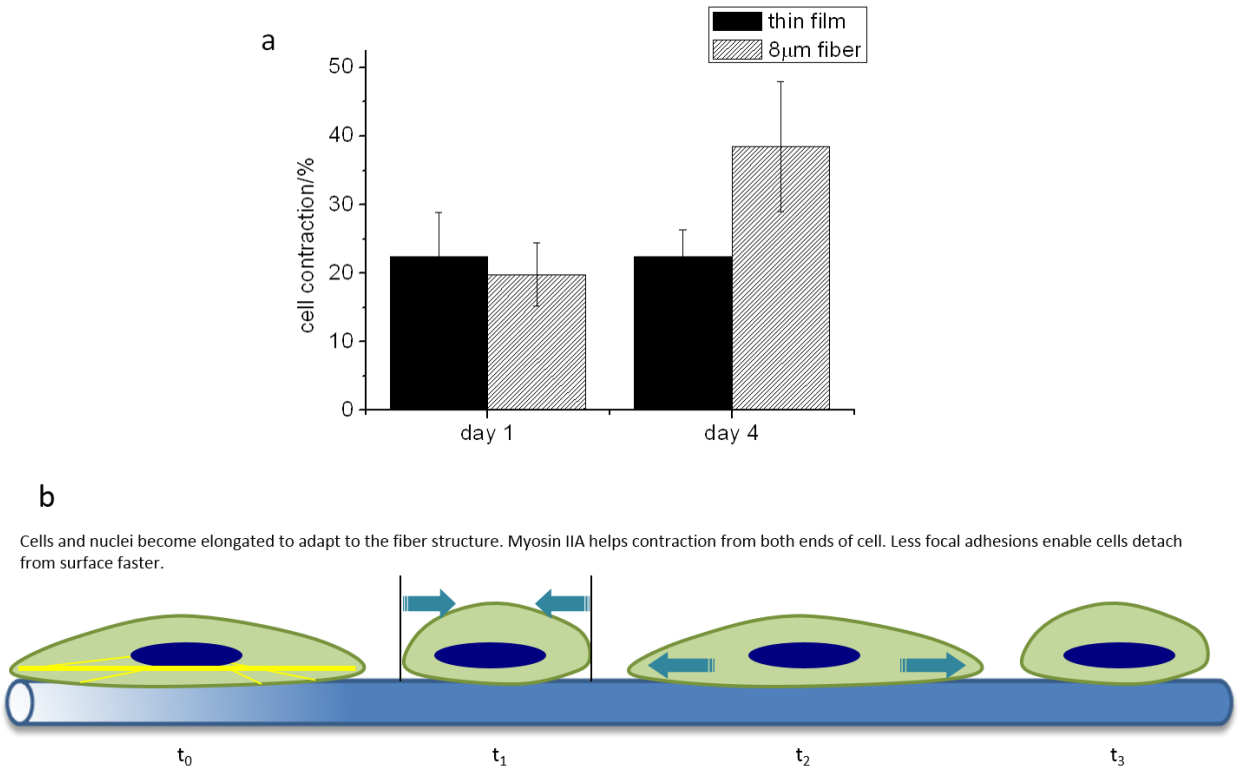

Figure 4.7 Cell contraction associated with migration on thin film and 8μm fiber - (a) Measurement of cell contraction on micron fibers and flat films at day 1 and day 4. Cell contraction on micron fiber is defined as: (cell length at t0- cell length at t1)/cell length at t1. (b) Illustration of cell contraction when migration on 8μm fibers at day 4.

4.4 Discussion

Cell migration on fibrillar substrates appears to differ in a fundamental fashion from migration on planar surfaces. Since cells rarely migrate on flat planes in vivo, it is important to understand the changes induced on fibrillar surfaces. Two types of surfaces were prepared for these experiments, a flat spun cast PMMA film and 8μ

diameter electrospun fibers. Both types of surfaces are not particularly cell adhesive, and therefore they were coated with fibronectin for 2 hours prior to plating the cells or the cell laden droplets. Hence the surfaces had identical chemical composition, but differed mostly in topography. On the flat surface the cells emerged en-mass from the droplet in a star burst trajectory with a velocity that decreased over the next 24 hours to the single cell value, as the cells separated. This value remained unchanged over the next seven days. For droplets placed on the fibrillar surfaces, the cells emerged only along the fibers. Careful examination indicated that most of the cells were attached on one side to the edge of the fibers with the other side of the cell on the adjacent flat surface. Immunohistochemical staining of vinculin proteins showed that on the fiber surfaces, the majority of the focal adhesions were concentrated in a straight line along the contact area with the fiber and along the periphery of the cell adherent to the flat surface. Very few focal adhesions were detected in the center of the cell. On the flat surfaces, on the other hand, even though some focal adhesions were seen along the leading and trailing edges, focal adhesions were distributed throughout the cell's plasma membrane. As a result cells on flat surfaces had approximately 40% more focal adhesions after 24 hours. On the flat surfaces the number remained constant, while on the fibrillar surfaces they decreased by approximately 30% on day 4.

Focal adhesions are also responsible for anchoring the actin fibers and transmission of traction forces across the cytoplasm. Pan et al. [18] had shown that the distribution of the traction forces was also responsible for causing nuclear deformation, and initiating cellular translocation. Hence I postulated that the differences in focal adhesion distribution would also results in differences in the traction forces exerted and

hence migration velocities and modes of cellular locomotion. Measurements of the cell migration velocity indeed showed that while the migration velocity remained constant on the flat surfaces, the velocity increased, nearly doubling, over the next four days for the cells on the fibrillar surface. This increase mirrored the decrease in focal adhesions, possibly enabling the faster motion. Another interesting observation though was the difference in nuclear deformation. The mean deformation on the fibrillar surfaces was nearly twice as large as on the flat surfaces, which was consistent with previous reports where cells were confined in porous substrates and migration was interrupted when the degree of confinement prevented nuclear deformation [18]. Furthermore, the nuclear deformation increased between days one and four, also mirroring the increase in cell migration velocity.

Observation of the mode of migration also showed differences between the flat and the fibrillar surfaces, where the differences were initially small on day 1, but increased and became very noticeable by day 4. On the flat surfaces migration was accompanied by a series of fluid deformations of the cytoplasm due to extension of lamellipodia, nuclear deformation and retraction of the rear of the cell. This mechanism was also observed initially on the fibers, on the first day, when the magnitude of the speed for cells migrating on both surfaces was similar. As the cells accelerated over the next three days on the fibrillar surfaces a different mode of migration started to spread. The cytoplasm contracted and expanded, in a manner similar to muscle cells, while the nucleus remained highly deformed. While RT-PCR and immunofluorescence indicated that the amount of myosin did not change for the cells on the fibrillar surface during the four day observation period, immunofluorescence images showed that large

myosin/actin fibers had formed. Measurements of the cell contraction also showed that during this time the contraction amplitude doubled for cell migrating on the fibers, while remaining unchanged for those migrating on the flat surface, suggesting that these larger fibers, were more efficient at contracting the cells.

Taken together, these results indicate that the continual deformation of the cells imposed by the fiber topography was responsible for triggering a different mode of migration, which is more oriented, faster, and more efficient than that observed on flat surfaces.

4.5 Reference

[1]. Grinnell F, Rocha LB, Iucu C, Rhee S, Jiang H Nested, collagen matrices: a new model to study migration of human fibroblast populations in three dimensions. Exp Cell Res, 2006, 312: 86-94.

[2]. Grinnell F, Fibroblast biology in three-dimensional collagen matrices. Trends Cell Biol, 2003, 13: 264-249.

[3]. Grinnell F, Fibroblasts, myofibroblasts, and wound contraction. J Cell Biol, 1994, 124: 401–404.

[4]. Grinnell F, Petroll WM, Cell motility and mechanics in three-dimensional collagen matrices. Annu Rev Cell Dev Biol, 2010, 26: 335-361.

[5]. Watterson KR, Lanning DA, Diegelmann RF, Spiegel S, Regulation of fibroblast functions by lysophospholipid mediators: potential roles in wound healing. Wound Repair Regen, 2007, 15: 607-616.

[6]. Schultz GS, Wysocki A, Interactions between extracellular matrix and growth factors in wound healing. Wound Repair Regen, 2009, 17: 153-162.

[7]. Jeon H, Hidai H, Hwang DJ, Healy KE, Grigoropoulos CP, The effect of micronscale anisotropic cross patterns on fibroblast migration. Biomaterials, 2010, 31: 4286-4295.

[8]. Kaiser JP, Reinmann A, Bruinink A, The effect of topographic characteristics on cell migration velocity. Biomaterials, 2006, 27: 5230-5241.

[9]. Berry CC, Campbell G, Spadiccino A, Robertson M, Curtis AS, The influence of microscale topography on fibroblast attachment and motility. Biomaterials, 2004, 25: 5781-5788.

[10]. Doyle AD, Wang FW, Matsumoto K, Yamada KM, One-dimensional topography underlies three-dimensional fibrillar cell migration. J Cell Biol, 2009, 184: 481-490.

[11]. Sheets K, Wunsch S, Ng C, Nain AS (2013) Shape-dependent cell migration and focal adhesion organization on suspended and aligned nanofiber scaffolds. Acta Biomater 9: 7169-7177.

[12]. Wang HB, Mullins ME, Cregg JM, McCarthy CW, Gilbert RJ, Varying the diameter of aligned electrospun fibers alters neurite outgrowth and Schwann cell migration. Acta Biomater, 2010, 6: 2970-2978.

[13]. Liu Y, Franco A, Huang L, Gersappe D, Clark RA, et al. Control of cell migration in two and three dimensions using substrate morphology, Exp Cell Res, 2009, 315: 2544-2557.

[14]. McClain SA, Simon M, Jones E, Nandi A, Gailit JO, et al. Mesenchymal cell activation is the rate-limiting step of granulation tissue induction. Am J Pathol, 1996, 149: 1257–1270.

[15]. Huttenlocher A, Horwitz AR, Integrins in Cell Migration. Cold Spring Harb Perspect Biol, 2011, 3: a005074

[16]. Singer II, Kawka DW, Scott S, Mumford RA, Lark MW, The fibronectin cell attachment sequence Arg-Gly-Asp-Ser promotes focal contact formation during early fibroblast attachment and spreading. J Cell Biol, 1987, 104: 573-584.

[17]. Kim DH, Wirtz D, Focal adhesion size uniquely predicts cell migration. FASEB J, 2013, 27: 1351-1361.

[18]. Pan Z, Ghosh K, Liu Y, Clark RA, Rafailovich MH, Traction stresses and translational distortion of the nucleus during fibroblast migration on a physiologically relevant ECM mimic. Biophys J, 2009, 96: 4286-4298.

[19]. Wolf K, Te Lindert M, Krause M, Alexander S, Te Riet J, et al. Physical limits of cell migration: Control by ECM space and nuclear deformation and tuning by proteolysis and traction force. J Cell Biol, 2013, 201: 1069-1084.

[20]. Wang N, Tytell JD, Ingber DE, Mechanotransduction at a distance: mechanically coupling the extracellular matrix with the nucleus. Nat Rev Mol Cell Biol, 2009, 10: 75-82.

[21]. Friedl P, Wolf K, Lammerding J, Nuclear mechanics during cell migration. Curr Opin Cell Biol, 2011, 23: 55-64.

[22]. Lombardi ML, Jaalouk DE, Shanahan CM, Burke B, Roux KJ, et al. The interaction between nesprins and sun proteins at the nuclear envelope is critical for force transmission between the nucleus and cytoskeleton. J Biol Chem, 2011, 286: 26743-26753.

[23]. Heissler SM, Manstein DJ, Nonmuscle myosin-2: mix and match. Cell Mol Life Sci, 2013, 70: 1-21.

[24]. Jorrisch MH, Shih W, Yamada S, Myosin IIA deficient cells migrate efficiently despite reduced traction forces at cell periphery. Biol Open, 2013, 2: 368–372.

[25]. Shih W, Yamada S, Myosin IIA dependent retrograde flow drives 3D cell migration. Biophys J, 2010, 98: L29-31.

[26]. Cai Y, Rossier O, Gauthier NC, Biais N, Fardin MA, et al. Cytoskeletal coherence requires myosin-IIA contractility. J Cell Sci, 2010, 123: 413-23.

[27]. Swailes NT, Colegrave M, Knight PJ, Peckham M, Non-muscle myosins 2A and 2B drive changes in cell morphology that occur as myoblasts align and fuse. J Cell Sci, 2006, 119: 3561-3570.

[28]. Tamada M, Perez TD, Nelson WJ, Sheetz MP, Two distinct modes of myosin assembly and dynamics during epithelial wound closure, J Cell Biol, 2007, 176: 27–33.

[29]. Fomproix N, Percipalle P, An actin-myosin complex on actively transcribing genes. Exp Cell Res, 2004, 294: 140-148.

[30]. Pasapera AM, Schneider IC, Rericha E, Schlaepfer DD, Waterman CM , Myosin II activity regulates vinculin recruitment to focal adhesions through FAK-mediated paxillin phosphorylation. J Cell Biol, 2010, 188: 877-90.

[31]. Chen, CS, Separate but not equal: Differential mechanical roles for myosin isoforms. Biophys J, 2007, 92: 2984-2985.

[32]. Vicente-Manzanares M, Ma X, Adelstein RS, Horwitz AR, Non-muscle myosin II takes centre stage in cell adhesion and migration. Nat Rev Mol Cell Biol, 2009, 10: 778-90.

[33]. Doyle AD, Kutys ML, Conti MA, Matsumoto K, Adelstein RS, et al. Micro-environmental control of cell migration--myosin IIA is required for efficient migration in fibrillar environments through control of cell adhesion dynamics. J Cell Sci, 2012, 125: 2244–2256.

[34]. Rossier OM, Gauthier N, Biais N, Vonnegut W, Fardin MA, et al. Force generated by actomyosin contraction builds bridges between adhesive contacts. EMBO J, 2010, 29: 1055-1068.

Chapter 5 The role of substrate mechanics in pluripotency preservation and proliferation of Notch induced cord blood CD34+ HSCs

5.1 Introduction

Hematopoietic stem cells (HSCs) are rare cells capable of differentiating into all three blood lineages identified in bone marrow and liver, umbilical cord blood, and peripheral blood. HSCs are used in clinical transplantation protocols to treat a variety of diseases [1, 2]. Although bone marrow transplantation has been applied clinically for more than three decades, the use of HSCs remains limited due to the difficulty in finding matching donors and limited ability to expand these cells ex vivo [3-7]. The biggest challenge is to maximize HSCs expansion without impairing their pluripotency.

Notch is a critical signaling pathway in the HSCs niche, and has the potential to increase ex vivo cord blood cell expansion [8-14]. Besides biochemical factors, the mechanics and biophysical cues can also affect stem cell proliferation [15-20]. Hydrogels are low cost, easily produced, biocompatible substrates, whose moduli are easily controlled by varying the degree of cross-linking [21-25]. Here I demonstrate that a synergy can be achieved between Notch signaling and hydrogel mechanics to successfully expand and maintain stemness of HSCs over a short culture period.

5.2 Materials and Methods

5.2.1 Hydrogel substrates preparation

Hydrogels were prepared with microbial transglutaminase (mTG) cross-linked gelatin. 0.1g/ml (10 %(w/v)) gelatin was first dissolved in DPBS at 70-80oC and filtered through 0.22 μm SteriFlip media filters. After sitting at room temperature overnight,

gelatin was then mixed with sterilized 0.1g/ml (10 %(w/v)) mTG which acted as a cross-linker. Two different ratio solutions yielded hard (gelatin: mTG=3:1) and soft (gelatin: mTG=125:1) hydrogels respectively. Solutions were then incubated at 37oC for 24hrs followed by a re-heating at 65oC for 5-7 min to deactivate mTG.

5.2.2 Stem cell culture

Human cord blood CD34+ cells were purchased from AllCells LLC and cultured in StemSpan SFEM media, 10% FBS, 100 ng/ml each of human SCF, TPO, and Flt-3L. Cells were infected with ICD-Notch or GFP control lentiviral particles then plated on hydrogels for 6 days. The cells were then counted and stained for CD34 and CD38 for flow cytometry.

5.2.3 Proliferation and phenotype detection

Samples were also viewed under a MetaMorph®-operated CoolSNAP™HQ camera attached to a Nikon Diaphot-TMD inverted microscope fitted with a 37 °C incubator stage, where time-lapse images were taken automatically. SMFM were used to measure the cell modulus on different hydrogels. CFU assays were carried out as per the manufacturer's protocol on 6-day old NOTCH-induced HSCs grown on soft hydrogels. The NOTCH-induced HSCs were plated in MethoCult and observed for CFU colonies.

5.3 Results and discussion

5.3.1 Organization of stem cell on different substrates

In figure 5.1a-5.1c, the phase-contrast images of the cord blood HSCs after incubation on the two types of hydrogels and untreated cell culture petri dish (TCP) showed diverse cell growth patterns. The cells have agglomerated on both types of gels into a central pellet of densely packed cells, whereas in the control dish, they are randomly dispersed throughout the dish. Closer examination also indicated differences in the appearance of the pellet for the hard and soft gels. On the hard gel (Figure 5.1b), the edge of the pellet is diffuse and small clusters of cells were present which have nucleated outside the main pellet. In contrast, the edges of the pellet on the soft hydrogels were sharp and well ordered (Figure 5.1c). The insets in figures 1b and 1c showed a larger magnification image of the cells in the interior of each pellet. The cells on the softer hydrogel displayed an ordered nearly perfect hexagonal close packed structure, whereas multiple defects in the packing are observed on the harder gel.

The structure of the pellets was similar for transduced and non-transduced cells, but the influence of the substrate adhesion became apparent immediately. It was previously shown by Pan [26] et al that adherent dermal fibroblast cells exert traction forces which deform hydrogels. Since the HSCs have much smaller adhesion forces than dermal fibroblasts, they also exert lower traction forces, and hence prefer softer gels, which are more susceptible to deformation. This ability to sense the local structure becomes apparent in the images of the cells approaching the edge of the pellet. In the case of the softer gels, cells formed small adjustments as the edge was approached

and then fit in perfectly into the hexagonal close packed structure. On the harder gels, the cell motion was more random as the edge was approached and it appeared to be more difficult for the cells to maintain an organized structure.

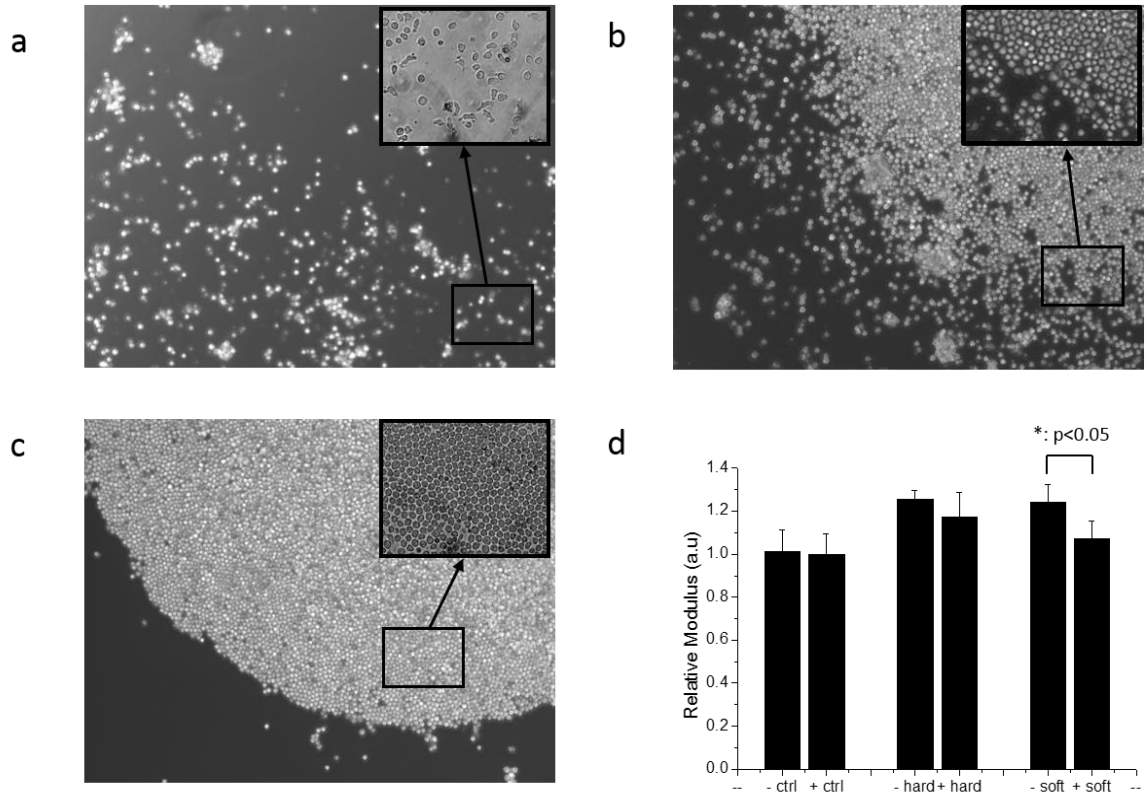

Figure 5.1 Dispersion and cell modulii of HSCs at day 6. (a) Phase-contrast images (25x) of HSCs cultured on control tissue culture petri dish (TCP), (b) HSCs cultured on hard hydrogel, and (c) HSCs cultured on soft hydrogel. (d) HSCs modulii on TCP (control), hard and soft hydrogels with transduced (+) and non-transduced (-) HSCs at day 6. *p< 0.05 on soft hydrogel.

5.3.2 Cell modulus

In order to determine whether the HSCs were able to interact and respond to their culture environment, the relative modulii of the cells were recorded on hydrogel surfaces and TCP +/- notch (Fig. 1d). I demonstrated that transduction with Notch did not have any effect on the modulii of cells plated on the TCP. It is interesting to note that the modulii of the cells plated on the soft hydrogels are slightly larger than those of the cells on the much harder TCP, suggesting partial adhesion was occurring. In the absence of notch, the modulii of the HSCs were insensitive to the mechanics of the gel, whereas the transduced cells were significantly softer on the soft gels compared to the hard ones. This indicated that in the presence of Notch, the HSCs were responding to the mechanics of the substrate.

5.3.3 HSCs expansion ex-vivo

In order to examine the possible synergistic effects of overexpressing Notch in HSCs coupled with cell culture on hydrogels, I plated transduced (+) and non-transduced (-) cells on TCP, hard, and soft hydrogel substrates. After six days of incubation, I saw a large difference in the number of cells (246750cells/well) for the HSCs with Notch overexpression and grown on a soft hydrogel (Fig. 5.2a), following an initial plating of the same number of cells, 10000 in each well. Overexpression of notch increased the number of cells by nearly a factor of two on both TCP and hard hydrogel, while a greater than 5-fold increase was observed on the soft hydrogel.

As shown in the modulus data, only the transduced cells were able to differentiate between the modulii of the underlying gel substrates and adjust their modulii

accordingly. It has previously been shown that cell proliferation could be a function of substrate modulus [27]. In the case of dermal fibroblasts, which are responsible for gel contraction and hence are callable of exerting large traction forces, the proliferation rate was larger on hydrogels with higher modulii. HSC adhere only weakly, and the traction forces which they are capable of exerting are much weaker. Hence in order to organize and sense gradients produced by other cells, they may prefer more deformable substrates. Furthermore, since cell division also involves exertion of traction forces, proliferation may be more favorable on the softer substrates. From figure 5.2a I find that expression of Notch alone is responsible for an increase in nearly a factor of two on both control and hard hydrogels. On the soft hydrogel, an increase of nearly a factor of 5 is observed when notch is introduced. This data shows that a resonance can result when both factors favoring proliferation are present, where the combined effect is much larger than the individual enhancements.

5.3.4 Preservation of HSCs pluripotency

In order to identify if the combination of the overexpression of Notch and utilizing an mTG-hydrogel had an effect on the pluripotency preservation, similar experiment was conducted and cells were then labeled with CD34 and CD38 markers. The flow cytometry results of +/- Notch on three different substrates are shown in figure 5.2b. I find that the amounts of progenitor and stem cells were not significantly affect by the addition of Notch on both control and hard gel surfaces, while on the other hand a large enhancement is observed on the soft hydrogel. Hence the increase in proliferation is not associated with increased differentiation. It is contrast to previous works where

substrate mechanics was shown to induce differentiation along multiple lineages, [28, 29] and in this case I find that mechanics can also be an important factor in preservation of stemness. These results underscore the important role that mechanics plays in the control of stem cell fate within the stem cell niche.

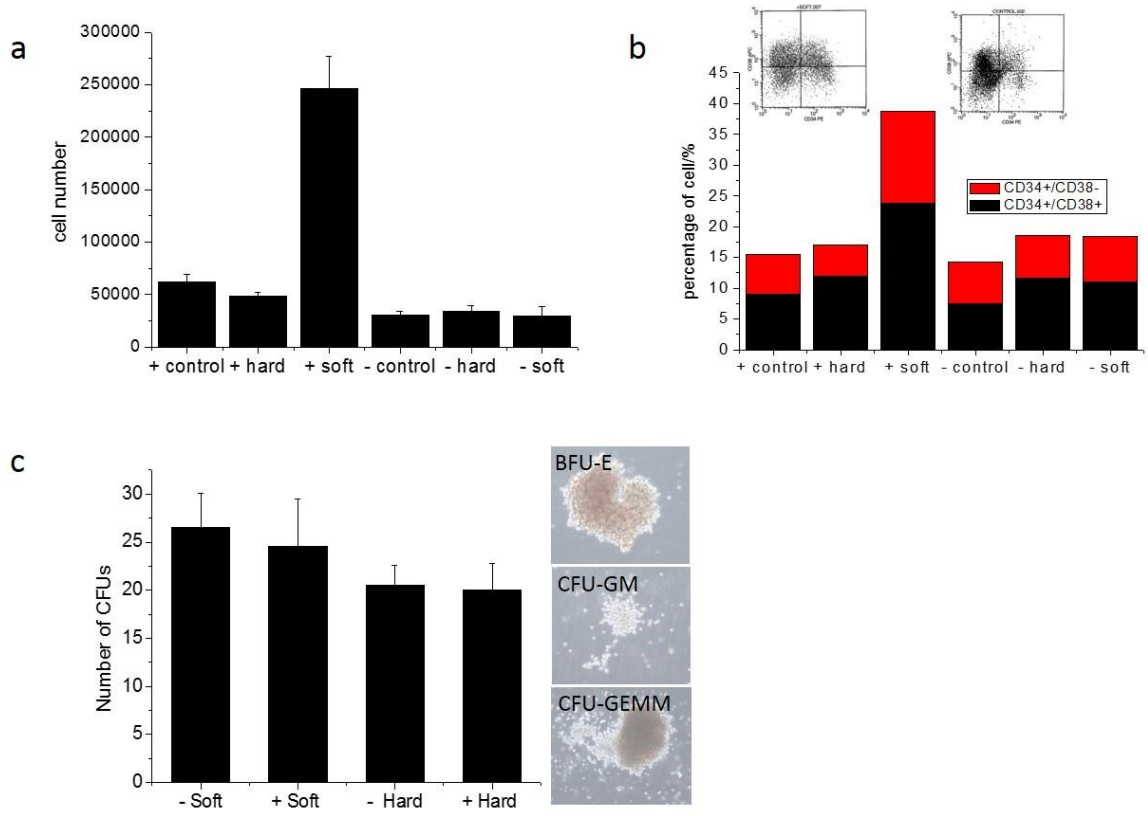

Figure 5.2 Proliferation and pluripotency tests of HSCs. (a) cell count on TCP (control), hard and soft hydrogels with transduced (+) and non-transduced (-) HSCs at day 6 with an initial 10000 cells per well. (b) flow cytometry result at day 6 on the same samples. (c) CFU assays of NOTCH-transduced HSCs cultured on soft hydrogels and phase contrast images (40x) of BFU-E, CFU-GM, and CFU-GEMM colonies.

5.3.5 Downstream CFU test

In order to demonstrate the Notch-induced cells had the capacity to differentiate into various lineages, CFU assays were conducted. Various CFU colonies were able to differentiate from NOTCH-induced HSCs grown on soft hydrogels (Fig. 5.2c). Numerous lineages were observed in CFU assays using the NOTCH-induced HSCs, including BFU-E, CFU-GM, and CFU-GEMM colonies (40×) (Fig. 5.2c). These data demonstrated that the HSCs transduced with NOTCH and cultured on soft hydrogels were capable of differentiating into different blood cell lineages.

A culture system that closely recapitulates marrow physiology is essential to study the niche mediated regulation of hematopoietic stem cell fate at a molecular level [30-32]. It has previously been demonstrated how substrate mechanics can be tuned to determine differentiation linage [28, 29]. Here I focused on the role of mechanics in preserving stemness and enabling proliferation. This illustrated the complex interactions that occur between stem cells and their microenvironment, where a synergy of multiple factors was required to affect a dramatic increase in both proliferation and maintenance of stemness. I believe our ICD-Notch-transduced stem cells combined with an mTG crosslinked hydrogel may serve as the foundation for further success in ex vivo expansion of HSCs.

The results in this thesis showed that the surface topography, chemistry, and mechanics all played critical roles in interacting and influencing biological systems, and they provided a novel aspect in designing biomaterials whose property could be precisely engineered for different applications.

5.4 References

[1] Aguila JR, Liao W, Yang J, Avila C, Hagag N, Senzel L, Ma Y, SALL4 is a robust stimulator for the expansion of hematopoietic stem cells, Blood, 2011, 118: 576-585.

[2] Aguila JR, Mynarcik DC, Ma Y, SALL4: finally an answer to the problem of expansion of hematopoietic stem cells? Expert Rev Hematol, 2011, 4: 479-481.

[3] Brunstein CG, Barker JN, Weisdorf DJ, DeFor TE, Miller JS, Blazar BR, McGlave PB, Wagner JE, Umbilical cord blood transplantation after nonmyeloablative conditioning: impact on transplantation outcomes in 110 adults with hematologic disease, Blood, 2007, 110: 3064-3070.

[4] Gluckman E, Rocha V, Arcese W, Michel G, Sanz G, Chan KW, Takahashi TA, Ortega J, Filipovich A, Locatelli F, Asano S, Fagioli F, Vowels M, Sirvent A,Laporte JP, Tiedemann K, Amadori S, Abecassis M, Bordigoni P, Diez B, Shaw PJ, Vora A, Caniglia M, Garnier F, Ionescu I, Garcia J, Koegler G, Rebulla P,Chevret S; Eurocord Group, Factors associated with outcomes of unrelated cord blood transplant: guidelines for donor choice, Exp Hematol, 2004, 32: 397-407.

[5] Ballen KK, Spitzer TR, Yeap BY, McAfee S, Dey BR, Attar E, Haspel R, Kao G, Liney D, Alyea E, Lee S, Cutler C, Ho V, Soiffer R, Antin JH, Double unrelated reduced-intensity umbilical cord blood transplantation in adults, Biol Blood Marrow Tr, 2007, 13: 82-89.

[6] 8. Barker JN, Weisdorf DJ, DeFor TE, Brunstein CG, Wagner JE, Umbilical cord blood (UCB) transplantation after non-myeloablative (NMA) conditioning for advanced

follicular lymphoma, mantle cell lymphoma and chronic lymphocytic leukemia: Low transplant-related mortality and high progression-free survival, Blood, 2005, 106: 813a-813a.

[7] Schuster JA, Stupnikov MR, Ma G, Liao W, Lai R, Ma Y, Aguila JR, Expansion of hematopoietic stem cells for transplantation: current perspectives. Exp Hematol Oncol, 2012, 1(12).

[8] Shigeru Chiba, Concise review: notch signaling in stem cell systems. Stem cells. 2006, 24: 2437-2447.

[9] Dahlberg A, Delaney C, Bernstein ID, Ex vivo expansion of human hematopoietic stem and progenitor cells, Blood, 2011, 117: 6083-6090.

[10] Delaney C, Heimfeld S, Brashem-Stein C, Voorhies H, Manger RL, Bernstein ID, Notch-mediated expansion of human cord blood progenitor cells capable of rapid myeloid reconstitution, Nat Med, 2010, 16: 232-6.

[11] Schuster JA, Stupnikov MR, Ma G, Liao W, Lai R, Ma Y, Aguila JR, Expansion of hematopoietic stem cells for transplantation: current perspectives. Exp Hematol Oncol, 2012, 1(12).

[12] Bigas A, Espinosa L. Hematopoietic stem cells: to be or Notch to be, Blood, 2012, 119:3226-3235.

[13] VanDussen KL, Carulli AJ, Keeley TM, Patel SR, Puthoff BJ, Magness ST, Tran IT, Maillard I, Siebel C, Kolterud Å, Grosse AS, Gumucio DL, Ernst SA, Tsai YH,Dempsey

PJ, Samuelson LC, Notch signaling modulates proliferation and differentiation of intestinal crypt base columnar stem cells, Development, 2012, 139:488-97.

[14] Zhang XB, Beard BC, Beebe K, Storer B, Humphries RK, Kiem HP, Differential effects of HOXB4 on nonhuman primate short- and long-term repopulating cells, Plos Med, 2006, 3: e173.

[15] Cosgrove BD, Gilbert PM, Porpiglia E, Mourkioti F, Lee SP, Corbel SY, Llewellyn ME, Delp SL, Blau HM, Rejuvenation of the muscle stem cell population restores strength to injured aged muscles, Nat Med, 2014, 20: 255–264.

[16] Holst J, Watson S, Lord MS, Eamegdool SS, Bax DV, Nivison-Smith LB, Kondyurin A, Ma L, Oberhauser AF, Weiss AS, Rasko JE, Substrate elasticity provides mechanical signals for the expansion of hemopoietic stem and progenitor cells, Nat Biotechnol, 2010, 28: 1123-1128.

[17] Kelly DJ, Jacobs CR, The Role of Mechanical Signals in Regulating Chondrogenesis and Osteogenesis of Mesenchymal, Stem Cells, 2010, 90: 75-85.

[18] Choi JS, Harley BA, The combined influence of substrate elasticity and ligand density on the viability and biophysical properties of hematopoietic stem and progenitor cells, Biomaterials, 2012, 33: 4460-4468.

[19] Fisher OZ, Khademhosseini A, Langer R, Peppas NA, Bioinspired materials for controlling stem cell fate, Acc Chem Res, 2010, 43:419-428.

[20] Smith JN, Calvi LM, Concise review: Current concepts in bone marrow microenvironmental regulation of hematopoietic stem and progenitor cells, Stem Cells, 2013, 31:1044-1050.

[21] Peppas NA, Hilt JZ, Khademhosseini A, Langer R, Hydrogels in biology and medicine: From molecular principles to bionanotechnology, Adv Mate, 2006, 18: 1345-1360.

[22] Gerecht S, Burdick JA, Ferreira LS, Townsend SA, Langer R, Vunjak-Novakovic G, Hyaluronic acid hydrogen for controlled self-renewal and differentiation of human embryonic stem cells, Proc Natl Acad Sci. U.S.A, 2007, 104: 11298-11303.

[23] Hahn MS, Miller JS, West JL, Three-dimensional biochemical and biomechanical patterning of hydrogels for guiding cell behavior, Adv Mater, 2006, 18: 2679–2684.

[24] Ye Z, Zhou Y, Cai H, Tan W, Myocardial regeneration: Roles of stem cells and hydrogels, Adv Drug Deliv Rev, 2011, 63:688-697.

[25] Prestwich GD, Hyaluronic acid-based clinical biomaterials derived for cell and molecule delivery in regenerative medicine, J Control Release, 2011, 155:193-199.

[26] Pan Z, Ghosh K, Liu Y, Clark RAF, Rafailovich MH, Traction Stresses and Translational Distortion of the Nucleus during Fibroblast Migration on a Physiologically Relevant ECM Mimic, Biophys J, 2009, 96: 4286-4298.

[27] Ghosh K, Ren XD, Sh XZ, Prestwich GD, Clark RAF, Fibronectin functional domains coupled to hyaluronan stimulate adult human dermal fibroblast responses critical for wound healing, Tissue Eng, 2006, 12: 601-613.

[28] Lee J, Abdeen AA, Zhang D, Kilian KA, Directing stem cell fate on hydrogel substrates by controlling cell geometry, matrix mechanics and adhesion ligand composition, Biomaterials, 2013, 34:8140-8148.

[29] Khetan S, Guvendiren M, Legant WR, Cohen DM, Chen CS, Burdick JA, Degradation-mediated cellular traction directs stem cell fate in covalently crosslinked three-dimensional hydrogels, Nat Mater, 2013, 12: 458-46.

[30] Hines M, Nielsen L, Cooper-White J, The hematopoietic stem cell niche: what are we trying to replicate? J Chem Technol Biotechnol, 2008, 83:421-443.

[31] Jiang J, Papoutsakis ET, Stem-Cell Niche Based Comparative Analysis of Chemical and Nano-mechanical Material Properties Impacting Ex Vivo Expansion and Differentiation of Hematopoietic and Mesenchymal Stem Cells, Adv Healthc Mater, 2013, 2: 25-42.

[32] Dellatore SM, Garcia AS, Miller WM, Mimicking stem cell niches to increase stem cell expansion, Curr Opin Biotechnol, 2008, 19: 534-540.

Appendix

Cell migration on nanoscale fibers

In this thesis I focused primarily on micron scale fibers, where I was able to propose models explaining the cell migration. Submicron fibers were studied as well, but the behavior of the cells on these fibers is not well understood. It is of note though that the response of the cells to nanofibers is significantly different from that to the micron fibers and hence these results are presented here, but without a model.

In figure Appendix 1a we show histochemical staining of vinculin in the focal adhesion points for dermal fibroblasts plated on 0.7 micron fibers incubated for four days. From the figure we can see that the cells do not align along the fiber directions. Fibroblasts typically have an aspect ratio of 4 when plated on a thin film, with the long axis being approximately 20-30 microns. As we showed in the previous chapters, the cells will orient along fibers whose diameters are four microns or larger, but orientation along fibers whose diameters are much smaller probably requires too much confinement. Rather on these fibers the cell tend to spread such that they contact multiple fibers and have an appearance similar to the cells plated on flat surfaces. The aspect ratio of the cells on nanofibers is plotted in figure Appendix 1b and compared to the aspect ratio of cells plated on microfiber and flat surfaces. The distribution of the focal adhesion points of the dermal fibroblasts plated on the submicron fibers is shown in Appendix 1c, where we could see that it appears more similar to that on the flat films, than the highly oriented placement of focal adhesions on the eight micron diameter fibers. The number of focal adhesions is plotted in figure Appendix 1d for 1 to 4 days after plating, where we see, and is intermediate between the number on the eight micron fibers and the flat films. More important though, we also see that the number of focal adhesions remains contestant in time over the next three days similar to the behavior of the cells on flat films and in contrast to the decrease in number observed on the eight micron fibers. Finally, in figure Appendix 2a we plot the migration speed of the dermal fibroblasts plated on the submicron fibers, together with those plated on flat films, oriented single layer scaffolds and scaffolds forming angles of 90 and 30 degrees. From the figure we conclude that the behavior of the cells on the two layer and one layer scaffolds are similar namely, they increase over a period of three days by nearly the same amount. The migration speed on the flat films remains constant, and the migration on the submicron films follows the pattern of the flat film, indicating that the diameter of the fibers, rather than the number of layers determines the functional dependence. The similarity of the functional form on submicron fibers reflects the similarity in the distribution of focal adhesion points.

In figure Appendix 2b we also plot the XTT for the cells migrating on the flat and fibrillar films. From the figure we find that no significant difference exists between the metabolic function of the cells on the eight micron fibers and those on the flat films. Yet the metabolic function of the cells on the submicron fibers is nearly twice that of the cells on the other substrates. On flat films the focal adhesions are clearly placed at the perimeter of the cells and are correlated to cell polarization in the direction of motion. On the eight micron fibers, the focal adhesions are located along the fibers and at the unction points and therefore are also correlated to the direction of motion. On the nanoscale fibers the focal adhesions seems to be randomly located

relative the direction of motion, hence it is possible that more energy exerted by the cells in finding a unique direction .

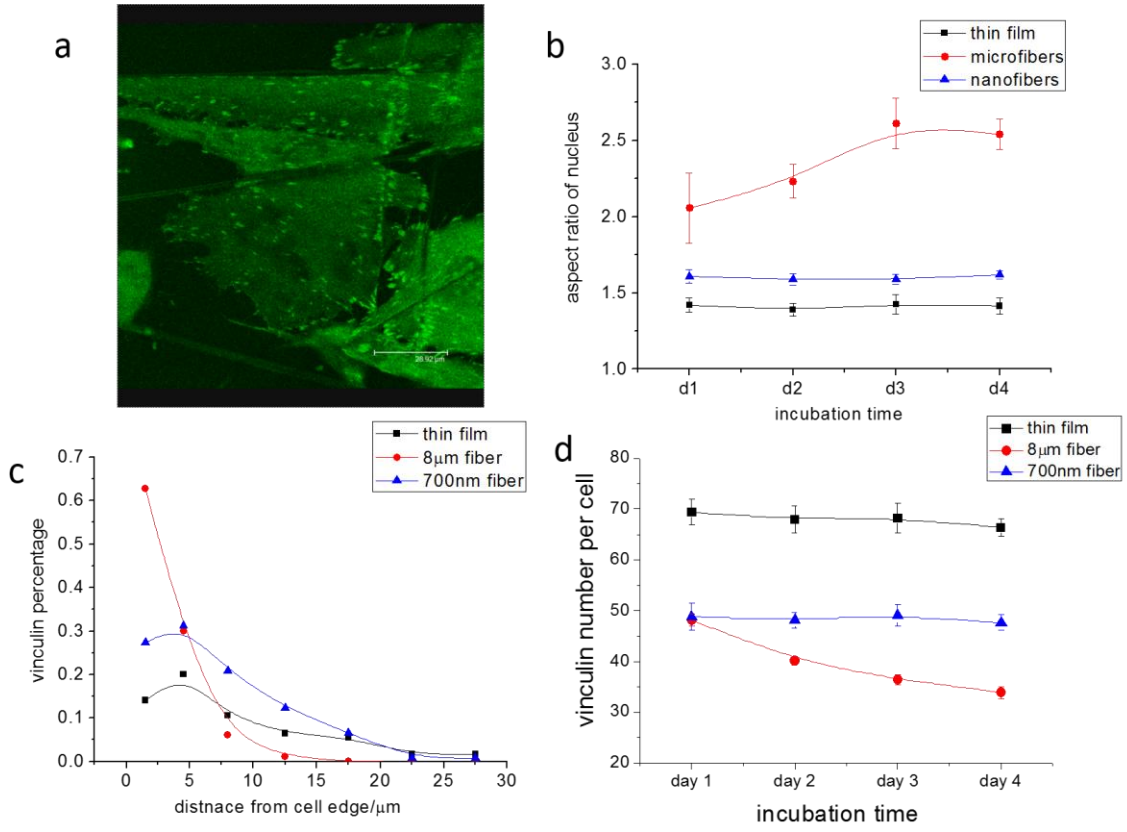

Figure Appendix 1. Focal adhesion and nuclear deformation on different substrates. (a) Immunofluorescent staining of vinculin on 700nm fibers. (b) Aspect ratio of nucleus, (c) Vinculin distribution, (d) Number of vinculin on thin film, microfibers, and nanofibers.

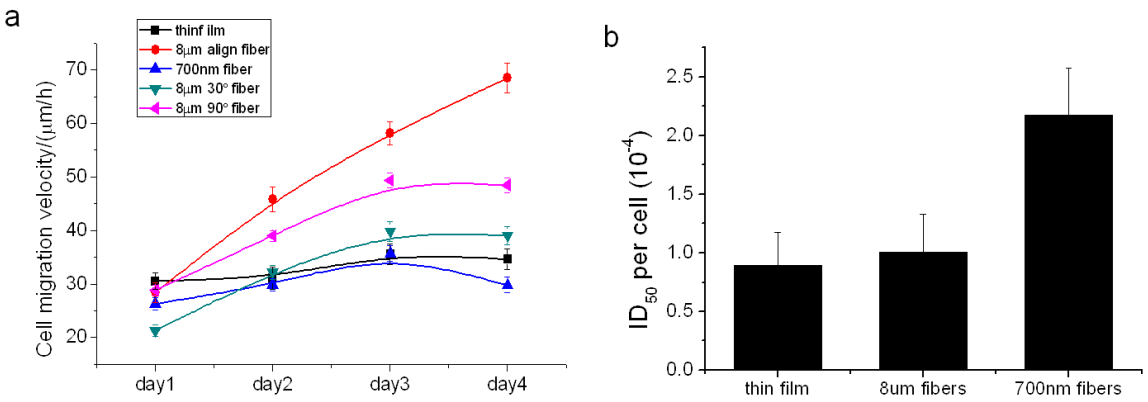

Figure Appendix 2. (a) Cell migration velocity on different surfaces. (b) XTT results on thin film, microfibers and nanofibers surfaces.